



Denoising of magnetic resonance images of brain tumor using BT-Autonet

Mamta Juneja ^{*}, Ashwani Rathee, Rishabh Verma, Raag Bhutani, Shashank Baghel, Sumindar Kaur Saini, Prashant Jindal ^{*}

University Institute of Engineering and Technology, Panjab University, Chandigarh, India



ARTICLE INFO

Keywords:
Denoising
Filtering
MRI
Autoencoder
Medical imaging
CAD

ABSTRACT

While obtaining medical images from sources such as Magnetic Resonance Imaging (MRI), Computed Tomography(CT), and ultrasound, noise is observed within images obtained from real world situations. Often this noise is caused due to vibrations of magnetic coils caused by quick electrical pulses, random thermal motion of protons in the tissue, reverberation and refraction artifacts. Denoising technique is one of the critical aspects in the Computer-aided Diagnosis (CAD) system, since MRI is susceptible to noises like Gaussian, Rician and Rayleigh. Traditional methods for MRI denoising are prone to challenges such as loss of information, loss caused during compression and retention of edge features. Hence, this paper presents a comparative analysis of various image denoising methods and hence, proposes an autoencoder based network Brain Tumor (BT)-Autonet for the removal of noise from brain MRI. Further, the performance analysis of the various denoising approaches is measured using different metrics. The proposed network BT-Autonet for 128×128 image dataset achieves a Peak Signal-to-Noise Ratio (PSNR) of 30.788, Mean Square Error(MSE) of 25.179, Structural Similarity Index Measure(SSIM) of 0.9 for Gaussian Dataset. It achieves a PSNR of 27.952, MSE of 23.129, SSIM of 0.861 for Rician Dataset and PSNR of 25.329, MSE of 44.378, SSIM of 0.873 for Rayleigh Dataset with an execution time of 10.5 s for Gaussian Dataset, 11 s for Rician Dataset and 11 s for Rayleigh Dataset. For 256×256 image dataset, BT-Autonet achieves a PSNR of 30.452, MSE of 30.036, SSIM of 0.816 for Gaussian Dataset while PSNR of 29.64, MSE of 41.684, SSIM of 0.809 for Rician Dataset and PSNR of 12.818, MSE of 67.219, SSIM 0.279 for Rayleigh Dataset with an execution time of 25 s for Gaussian Dataset, 27 s for Rician Dataset and 26 s for Rayleigh Dataset during the examination. Therefore, the proposed network outperformed the existing models in PSNR, SSIM, MSE and execution time.

1. Introduction

The acquisition of high-quality medical images is essential to support doctors in disease diagnosis. In medical image analysis, image quality is critical for diagnosis and therapy planning. Many techniques such as Magnetic Resonance Imaging (MRI), ultrasound, and Computed Tomography (CT) have been developed to acquire medical images. MRI has become the most precise and sought-after imaging technique because its resolution and methodology are inherently safe. MRI is a method that creates a detailed, distorted image of a body organ using radio waves and a strong magnetic field. It is a non-invasive and painless process that, unlike CT, does not expose the patient to hazardous X-ray radiation. The quality of MRI scanning is determined by the scanner's magnetic field strength, which can range from 0.5 to 3.0 T, with 1.5 T

being the normal clinical setting. 1.5 T magnetic strength produces a weaker signal than 3.0 T. 3.0 T has been shown to produce remarkably perfect and bright images by performing scans in a short period of time, reducing overall scan time. According to a study conducted in Japan, there are around 48 machines per 100,000 patients, making it the country with the most MRI scanners per capita. Different MRI sub-modalities, such as Dynamic Contrast Enhanced (DCE) MRI, Diffusion Weighted Imaging(DWI), T1-weighted and T2-weighted MRI, can also create Multiparametric MRI(mp-MRI) [1]. When compared to other imaging modalities like ultrasound and CT, MRI provides unique and valuable information. MRI can define and differentiate between benign (non-cancerous) and malignant (cancerous) tissues by using physical and biochemical characteristics. Creating comprehensive and contrast images of the organs, it aids clinicians in finding anomalies in the body

^{*} Corresponding authors.

E-mail addresses: mamtajuneja@pu.ac.in (M. Juneja), ashwanirathee.work@gmail.com (A. Rathee), rishabhverma132001@gmail.com (R. Verma), raagbhutani2002@gmail.com (R. Bhutani), cnctrashank@gmail.com (S. Baghel), sumindarkaursaini@gmail.com (S.K. Saini), jindalp@pu.ac.in (P. Jindal).

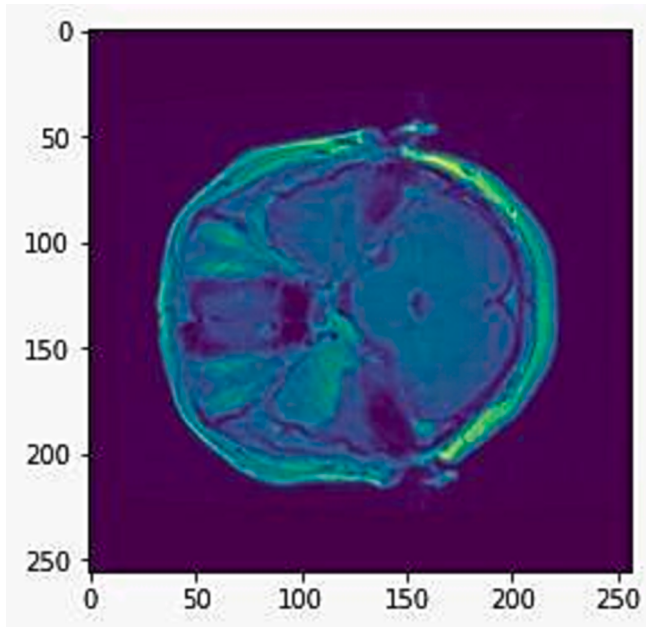


Fig. 1. MRI Scan with Brain Tumor.

with greater precision than other imaging modalities. It uses radio-frequency pulses to estimate the presence of a tumor in the target area [2]. However, during the acquisition of MRI, environmental and external conditions cause noises such as Gaussian and Rician in the images, resulting in fuzzy and incomprehensible details and possibly the loss of crucial features from the images. This could lead to a misdiagnosis, as well as issues in subsequent phases of medical image processing. As a result, the most difficult phase in the CAD system is preparing the image so that image segmentation and classification can be done more efficiently [3]. Because noise-free image data is necessary for efficient system operation, image denoising is crucial in a variety of applications, such as image restoration, image registration, image segmentation, and image classification. As a result, MRI denoising techniques are quite important to provide better visualization of abnormal parts of the body. Denoising the medical image is a particularly complex and challenging task. It is important to strike a balance between noise reduction and feature preservation that supports the diagnostically useful image content. Historically, one of the quality issues with image analysis has been reducing noise. The success of many analysis techniques like segmentation, and classification depends mainly on the image being noiseless, and this is usually done using a denoising process. Hence, denoising is an important preprocessing step to improve image quality by reducing noise components while preserving the characteristics of all images. CAD is a system that acts as an assisting tool for radiologists and doctors to provide precise visualization and automatic detection of the disease. It consists of mainly three stages; preprocessing, segmentation and classification. Preprocessing is the initial and most vital stage of the CAD system. In this stage, many researchers have employed different denoising techniques. Traditional denoising filters such as Mean filter, and Gaussian filter add the blurring effects in order to denoise the image. Traditional methods for MRI denoising are prone to challenges such as data loss owing to compression and preservation of edge information, which harms the performance of a conventional CAD system's segmentation and classification. Traditional approaches either over-smooth the image while removing noise or do not remove noise completely [3]. To overcome such problems, many autoencoder based approaches like Residual Dense Neural Network(RDUNet) [4] are used which promise significantly better results, in this research work an autoencoder based denoising technique is proposed for the MRI of Fig-share brain tumor dataset. The **Fig. 1** shows the MRI scan with brain

tumor.

1.1. Noises in MRI

MRI are susceptible to noises and some of them impact every pixel of the image. For denoising, it is important to learn the fundamental mathematical structure of the noise. In the following section Gaussian, Rician noise, Rayleigh noise, and salt and pepper noise in MRI are discussed.

1.1.1. Gaussian noise

It is a type of electronic noise caused by atomic thermal vibrations and other natural sources. This noise generally disrupts the gray values in images. That's the reason it is designed and attributed to its probability density function which is normally distributed [5]. The noise uses the divergent numbers as values for the probability distribution analysis when dispersed in a Gaussian manner.

$$pG(z) = \frac{1}{\sigma\sqrt{2\pi}} e^{\frac{-(z-\mu)^2}{2\sigma^2}} \quad (1)$$

In Eq. (1). z represents the gray level, whereas μ and σ represent the mean and standard deviation respectively.

1.1.2. Rician noise

The Rician distribution is the probability distribution of a circular bivariate ordinal random variable's value with a non-zero mean. Rician noise depends on the signal. The task of separating signals from noise is challenging. Low signal-to-noise ratio regimes are particularly challenging for Rician noise. In addition to introducing random fluctuation, it also lowers visual contrast by adding data with a signal-dependent bias. The images have both quantitative and qualitative degradation, which increases the likelihood of inaccuracy in the analysis [6].

It is represented as

$$f(v, \sigma) = \left(\frac{z}{\sigma^2}\right) \exp\left(-\frac{z^2 + v^2}{2\sigma^2}\right) I_0\left(\frac{zv}{\sigma^2}\right) \quad (2)$$

Here in Eq. (2), v and σ are shaped parameters of images z. When the pictures are damaged by Rician noise and experience a contrast-reducing signal dependent bias, an MRI restoration technique is employed. A correlated noise is created while the white noise acquisition time is shortened. The bias from the squared magnitude image is removed using a two step denoising technique, after which the square root of the image is determined [7].

1.1.3. Rayleigh noise

A continuous probability distribution for positive-valued random variables is the Rayleigh distribution. The noise can be visible within the range of radar and velocity of the image that's represented as Rayleigh distribution [8]. The probability density function of the Rayleigh noise is given as,

$$\begin{aligned} p(g) &= \frac{2}{b}(g-a)e^{-\frac{(g-a)^2}{b}} \text{ for } g \geq a \\ &= 0 \text{ for } g < a \end{aligned} \quad (3)$$

In Eq. (3), $a = \mu - \sqrt{\frac{\pi b}{4}}$ and $b = \frac{\sigma^2}{1-\frac{a^2}{\sigma^2}}$, $\mu = \text{mean}$ and $\sigma^2 = \text{variance}$

1.1.4. Salt and pepper noise

The black and white pixels in the image are referred to as salt and pepper noise. This noise is typically brought either by transmission problems or a lack of light exposure on the camera sensor. Salt and pepper noise does not completely destroy the image; instead, part of the pixel values is altered. For the scale of an 8-bit image, it is restricted to max and min intensity values, max value (salt) is 255 which appears as white pixels and for min value(pepper noise) is 0 which appears as black

pixels. By default, the faulty pixels are alternately assigned the maximum and minimum value, earning the names salt and pepper.[9].

The distribution of noise intensity is defined as:

$$P(N) = 0.5 P \text{ pepper}, N = 0$$

$$P(N) = 1 - P \text{ noise free pixels}, 0 < N < 255$$

$$P(N) = 0.5 P \text{ salt}, N = 255$$

Apart from the noises discussed above, there is a possibility of many more noises present in MRI, like speckle noise and impulse noise. During the design of an image denoising algorithm, prior understanding of the type of noise is critical to the method's efficacy and efficiency. Noises like salt and pepper noise, impulse noise, and speckle noise are essentially non-existent; they mostly occur due to faulty manufacturing of devices, a high photon count during image capture, and a high bit error rate; these noises do not affect the physical nature of the MRI. However, noises like Gaussian noise, Rician noise, and Rayleigh noise impact the entire image uniformly; it may be said that Gaussian noise influences practically every pixel of an image, which substantially limits the degree of visual interpretation. Therefore for better analysis of denoising methods Gaussian noise, Rician noise and Rayleigh noise are considered [10].

1.2. Contribution of the study

Noise is an undesirable signal that taints valuable and desirable information, for removal of these noises image denoising is the essential pre-processing process, which helps in order to recover the real image. Since edges, anatomical details, high frequency components, texture, and noise, are difficult to identify throughout the denoising process, the denoised images will necessarily lose some information. In the case of medical images, this loss of information makes the detection and analysis of diseases very complex and prone to error, resulting in significant losses, including fatalities.

- Although classical filters can remove the noise from the image, it results in various other alterations like uneven textures, blurred edges, and loss of data due to compression and prevention of edge details.
- CNN-based denoising approaches, which are based on the image degradation process, try to learn a mapping function by optimizing a loss function on a training set of degraded-clean image pairings, hence decreasing the alteration caused by the filters. However, because these neural networks are not perfect, they tend to lose part of the image's properties owing to image compression and decompression.
- The proposed model aims to reduce these losses by downsampling through convolutional strides rather than dropping some features while training.

The paper is further organized as: [Section 2](#) explaining state-of-the-art filters for denoising along with comparative analysis of the different techniques used for denoising, [Section 3](#) providing a literature survey of numerous noise removal techniques, [Section 4](#) includes proposed methodology of the paper; and [Section 5](#) comprises the experimental setup, datasets, performance metrics, and performance evaluation of the proposed approach. The section 6 discussed the performance and results of various state-of-the-art models with the proposed model along with their comparative graphical representation. Finally, [Section 7](#) concludes the paper while giving future scope.

2. State-of-the-art filters used for denoising

2.1. Median filter

A Median filter is a nonlinear filter that computes each output sample as the median value of the input samples within the window; the outcome is the middle value following the sorting of the input values. The "salt and pepper" noise in the image, or impulse noise, is effectively removed from this filter. Additionally, it helps in keeping the edges while minimizing random noise. Median filter also helps in reducing spiky noises and prevents the blurring of images [11]. Ellah et al. in 2016 proposed a CAD system in which preprocessing of images is done for reducing noise level and improving image quality. For this, the median filtering technique is used due to its efficiency in preserving the edges, smoothing spiky noises, and preventing the blurring of images [12]. Ahmed et al. in 2021 performed denoising using statistical methods to increase image quality. Denoising is done using the Median filter which shows the capability to preserve edges and overcome the issues of missing values in the image. After that data is augmented using rotation, scaling, reflection, translating, and cropping [13].

2.2. Wiener filter

A Wiener filter is used to reduce the amount of noise in a signal by comparing it to an estimate of the desired noiseless signal. Images with noise are cleaned up using a Wiener filter. The inner details of the image are protected while the sharp edges are softened by Wiener filters [14]. Hilal Naimi et al. (2015) proposed a denoising approach based on Dual Tree Complex Wavelets and Shrinkage with the Wiener filter technique (DTCWT). The study's outcomes demonstrated that denoised images using DTCWT with a Wiener filter are less redundant than Stationary Wavelet Transform(SWT) and have a better balance between smoothness and accuracy than DWT [15]. Mamta Mittal et al. in 2019 applied a Wiener filter on the normalized MRI as the basis of stationary wavelet transform to remove the noise and smooth the blurred images. The inner details of an image are also preserved. While the Wiener filter's PSNR is higher than the Anisotropic filter, it was discovered that the latter can also be used for the same purpose [16].

2.3. Gaussian filter

When filtering various types of surfaces, Gaussian filters are crucial. This kind of filtration is the first option for filtration in many applications due to the simplicity of the algorithm, simplicity of implementation, and robustness of the results. By convolving the measured surface with a Gaussian weighting function, Gaussian filters can be applied to the input surface. It is a low pass filter used for reducing noise (high-frequency components) and blurring regions of an image. The filter is implemented as an odd sized symmetric kernel which is passed through each pixel of the Region of Interest to get the desired effect. The kernel is not hard towards drastic color changes(edges) due to the pixels towards the center of the kernel having more weightage towards the final value than the periphery. By greatly reducing the sharpness of the image's edges, it effectively removes Gaussian noise. Hossain et al. in 2019, to increase MRI picture quality while minimizing the noise, employed a Gaussian blur filter to reduce Gaussian noise in brain MRI for better segmentation [17].

2.4. Total variational filter

The Total Variation (TV) is based on the energy function's minimization. It was specifically created to maintain sharp discontinuities in images while omitting noise and other undesirable fine scale detail. V. Nivitha Varghees et al. in 2012 proposed a total variational denoising algorithm. The standard deviation of noise in an MRI image is used to adapt the regularization parameter of the TV algorithm. Utilizing local

Table 1

Comparative Analysis of State-of-the-Art Filters.

S. No.	Filters	Pros	Cons
1.	Median Filter [12]	<ul style="list-style-type: none"> ● Reduce spiky noise ● Non linear filter ● Smoothens the image ● Prevent blur and preserve sharp edges 	<ul style="list-style-type: none"> ● Only better for removing salt and pepper noise
2.	Wiener Filter [14]	<ul style="list-style-type: none"> ● Conceptually simple ● Reduces speckle noise for big windows 	<ul style="list-style-type: none"> ● Restoration is challenging when there is random noise
3.	Gaussian Filter [17]	<ul style="list-style-type: none"> ● Effect for Gaussian noise ● Simplicity of algorithm is one of the pros 	<ul style="list-style-type: none"> ● Reduce the image details ● Unable to preserve edges
4.	Total Variation Filter [18]	<ul style="list-style-type: none"> ● Good for small value of SNR and able to preserve edges efficiently 	<ul style="list-style-type: none"> ● Denoised images would be blurry. ● Minimizes important details
5.	Wavelet Filter [19]	<ul style="list-style-type: none"> ● Regardless of the frequency composition of the signal, eliminate noise while keeping its properties 	<ul style="list-style-type: none"> ● Unable to preserve fine details in case of high noise data. ● There's a chance the wavelet coefficients are biased
6.	Bilateral Filter [22]	<ul style="list-style-type: none"> ● Better in preserving edges ● Effectively remove Gaussian noise 	<ul style="list-style-type: none"> ● Not the best fit for salt and pepper noise
7.	Anisotropic Filter [24]	<ul style="list-style-type: none"> ● Efficient in reducing Gaussian image 	<ul style="list-style-type: none"> ● Lowers the image resolution
8.	Non-local Mean Filter [25]	<ul style="list-style-type: none"> ● Preserve edges ● Better performance with redundant images 	<ul style="list-style-type: none"> ● Expensive, so non-suggestable for larger noise
9.	RDUNet [4]	<ul style="list-style-type: none"> ● Fast learning process 	<ul style="list-style-type: none"> ● Takes too much time to train

statistics, the noise standard deviation is calculated. Assessments for both objective and subjective visual quality conclude that proposed method is better in removing Rician noise than Nonlocal filter, Bilateral filter and multi-scale linear minimum mean square-error estimation [18].

2.5. Wavelet filter

Wavelet filter is used to denoise the images with Gaussian noise, which also have energy compaction properties. An impulsive, speckle and Gaussian noise-inclusive input signal is subjected to a wavelet transform before undergoing an inverse wavelet transform. During transformation, the noise is evenly distributed over all of the coefficients, but the bigger coefficients are where the most information is stored. The Discrete Wavelet transform (DWT) preserves the relevant information while removing the majority of the noise and spectrally characterizing the features. The filter's demerits include a lack of adaptivity, phase information, and computationally expensive operation [19].

Bing-quan-Chen et al. (2019) proposed a denoising method based on DWT and modified median filter, after comparing the results of the proposed network with the results of wavelet transform, median filter, contourlet etc. PSNR and Signal Noise Ratio(SNR) increased by 10%–15% for low noise images and 2%–6% increase in PSNR and SNR for high noise images.

These filters have broad applications in speech recognition, quantum physics, biometric security and fingerprint verification, signal processing, and other related domains [20].

2.6. Bilateral filter

Bilateral filter is a non-linear filtering technique to smooth images while retaining edges and textural features of the original image. It has various applications such as denoising, texture editing, and relighting. It is based on two inputs as size and contrast features. In this technique, each pixel is replaced by a weighted mean of its neighboring pixels by considering the value difference with the neighbors to maintain edges while smoothing [21]. This weight can be based on a Gaussian distribution. The fundamental Nilateral filter has the potential to add artificial edges to the image by introducing a reverse gradient effect. Due to the degradation caused to the edge values, this attribute renders it inappropriate for a variety of applications. Additionally, this filter introduces intensity plateaus that reduce the amount of information contained in the image. Mzoughi H et al. in 2019 applied a Bilateral filter to denoise MRI slices followed by a contrast stretching technique used to improve the contrast based on the MRI brain glioblastoma tumor's original statistical information. It removes Rician noise from uniform regions of White Matter (WM), Gray Matter (GM), and Cerebrospinal Fluid (CSF) while preserving the contours, structures, and the different subregion tumor boundaries such as tumor, necrosis, and edema [22].

Riji et al. in 2015 used nonlinear iterative bilateral filtering to remove Rician noise from an MRI. SNR and SSIM were two parameters that were used to assess the performance of the technique. Compared to other approaches, the method was found to effectively denoise images with significant edge details [23].

2.7. Anisotropic filter

This filter enhances the image quality while preserving the outer limits or edge of the image. The uniformly distributed noise gets reduced by using edge sharpening. Localization of linear diffusion filtering is done using a non-linear diffusion scheme. Image blur is avoided, and a second-order Partial Differential Equation (PDE) of heat provides a solution to this problem. When detection interacts better with edge detection, the results are better than the linear canny edge detector. Krissian et al. (2009) suggested removing Rician noise from MRI with an anisotropic diffusion filtering; a diffusion matrix was employed in place of a scalar in the partial differential equation in this case, which enhanced noise reduction. Additionally, the edge preservation performance of the linear filter is somewhat improved [24].

2.8. Non-local mean filter (NLM)

Non local Mean filter is another technique used for MRI denoising. It calculates the mean of all pixels in the image, weighted by the similarity of their neighborhoods to the target pixel, unlike “local mean” filters, which smooth the image by averaging the values of the pixels around the target pixel. This outputs the image of greater quality and minimum loss of detail in the MRI compared with the local means algorithm. Zhang et al. in 2014 claimed that the traditional Rician Non Local Mean (RNLM) filter generally blurs relevant small high-contrast particles. So, they proposed a novel RNLM-CPP algorithm using a combined patch and pixel similarity which can preserve small high-contrast particles better than the original RNLM algorithm [25]. Jian Yang et al. in 2015 proposed a Pre-Smoothing NLM (PSNLM) with transformed image based on NLM. In comparison, Gaussian pre-smoothing filters and Variance Stabilizing Transformations (VST) produce a better PSNR score [26].

2.9. Autoencoder

Autoencoder is an unsupervised artificial neural network, also known as an encoder-decoder network, used to learn data representations (encoding) into lower dimensions efficiently by training the network to eliminate the noise. Denoising autoencoders represent the stochastic version of autoencoder in which data is partially corrupted by

introducing noise to the input vector. Denoising autoencoders attempt to remove the noise from the noisy input and reconstruct the output similar to the original input. Tong Lu et al. (2021) proposed an autoencoder with an attention mechanism for denoising. The experimental results based on simulated real clinical images have shown that the proposed model is effective in reducing noise in MRI magnitude images and can achieve significant improvement in image quality as measured in terms of PSNR and SSIM. This is in contrast to the current mainstream denoising methods [27]. M.S. Hema et al. (2022) proposed a CNN with autoencoder based feature selection. Network consists of an autoencoder and CNN, an autoencoder used to eliminate noise and extract relevant features and CNN for classifying and prediction of tumors. The proposed method performed better than traditional CNN, decision tree, and bayesian classification [28].

The Table 1 represents the comparative analysis of state-of-the-art filters along with the pros and cons of each approach.

3. Literature survey

The denoising literature presents numerous noise removal techniques, discussions and denoising methods based on MRI medical images to preserve the optimal features and information of an image.

S. Suryanarayana et al. (2012) developed novel detection and filtering schemes for Gaussian noise. The proposed method shows better results in detecting and filtering Gaussian noise than the standard mean filter for various combinations of variances and mean of additive Gaussian noise [29]. Saritha Saladi et al. (2017) proposed Spatially Adaptive Non Local Mean (SANLM) filters which outperforms other conventional denoising methods both efficiently and effectively. This filter shows an improved PSNR of about 2.07% for denoised images. Bilateral filters perform the least in comparison to other filters. The MSE and Root-Mean-Square Error (RMSE) values decreased by a mean of 13.1% and 6.11%, and the SNR and SSIM metrics are optimized by an average of 7.20% and 2.32% for the denoised MRI [30]. Worku Jifara et al. (2017) proposed the deep CNN model for denoising of medical images for small training datasets as there are many denoising methods but they are only efficient for large training datasets. In the proposed method, residual learning learns the noise from noisy images. Batch Normalization integrates with residual learning to improve denoising performance and speeds up training time. For a small training dataset, the proposed method performs better than some of the existing models [31]. S. Agarwal et al. (2017) compare the efficiency of wavelet-based thresholding techniques for denoising the MRI in presence of speckle noise. Based on quantitative analysis of parameters like PSNR, SNR, MSE and visual quality of MRI, Symlet transform performs better than Morlet transform, Haar Transform and Daubechies Transform [32]. Ki Hwan Kim et al. (2018) in their paper generated HR and MRI in different contrast from downsampled MRI, using HR MRI; in contrast their metrics are Normalized Mean Square Error (NMSE) 0.009, 0.007 respectively on random sampling and central sampling. The proposed method outperformed the compressed sensing methods and the proposed method would be ideal for accelerating routine MRI scanning [33]. Shamima Nasrin et al. (2019) used the R2U-Net-based autoencoder model for medical image denoising. Performance of the R2U-Net encoder model is also tested for transfer domain between CT and MRI scans. The standard R2U-Net encoder model attained the output accuracy of 79.1% while the proposed model (without concatenation between encoding and decoding) attained 79.9% accuracy [34]. Xuexiao You et al. (2019) proposed a way for removing Rician-noise-perturbed MRI, an effective deep and wide CNN was used. For boosting the denoising presentation, a feedforward network that integrates residual learning and Batch Normalization (BN) is used to accelerate the training procedure. For this paper, the author uses a small training dataset and the results of the proposed denoising models are better than existing denoising techniques currently used in T1W MRI denoising. According to the paper, two main reasons for excellent denoising: first is smaller

intervals have a better denoising effect than the whole interval and the second is deep CNN architectures [35]. Hemalata V. Bhujle et al. (2019) categorized the numerous NLM based MRI based denoising techniques as fast NLM, adaptive NLM, multiresolution, and statistical based NLM techniques and their advantages and limitations are thoroughly discussed in the paper. And none of the methods attains good results in noise reduction and edge preservation [36]. Dibakar Sil et al. (2019) conclude that for noise distribution in noisy images inception -v3 performs better than VGG- 16, CNN architecture Fast and Flexible Denoising Network (FFDNet) when trained separately for different classes of noise distribution it attains 16% improvement in PSNR in comparison to blind denoising. From this study, it is suggested that if PSNR values are below 30 dB, a specific CNN network will be useful for detecting the type of noise distribution [37]. Dan Hong et al. (2020), Free-Fiber Architecture Diffusion Magnetic Resonance Imaging (FFA-DMRI), a feature fusion, and attention network, is proposed to separate the noise from MRI. A spatial attention mechanism has been designed to obtain the area of interest in MRI. FFA-DMRI is trained on the ADNI dataset. From analysis, it can be seen that FFA-DMRI can effectively remove Rician noise while maintaining the crucial details [38]. Bhawna Goyal et al. (2020) review various denoising methods and divide them into five categories, spatial domain methods, dictionary learning methods, methods in statistical domains, hybrid methods, and sparse representation and transform domain methods. Improved NLM filter performs well in the spatial domain, for transfer domain transform with overcomplete basis functions, increased number of scales, direction, and orientation generated better results. Multi-resolution based algorithms work better than single-resolution ones. It is observed that a single denoising algorithm might not be completely efficient for denoising; every method has its advantages and disadvantages so it was suggested to use a combination of various methods to utilize the attributes of different domains while overcoming the limitations [39]. Miao Tian et al. (2021) presented a conditional Generative Adversarial Network (GAN) based approach for MRI denoising. The proposed method attained better results in terms of denoising, SSIM, and robustness [40]. S. Ramesh et al. (2021) proposed a modified iterative groping median filter for the removal of salt and pepper noise and Maximum Likelihood Estimation (MLE) -based Kernel Principal Component Analysis (KPCA) is proposed for feature selection. The proposed technique shows better results from the state-of-the-art techniques, 25% better PSNR score, 10% increment in SSIM, and 8.83% enhancement in accuracy [41]. Divya Pankaj et al. (2021) proposed a method VMD-TV is based on Variational Mode Decomposition (VMD) for removing Rician noise, it consists of two stages first high-frequency modes from the image are discarded and the denoised image is then reconstructed from low-frequency modes and in second stage total variation image smoothing based on non-convex optimization is performed to reduce the remaining noise from the first stage. The results of the paper are based on a clinical dataset and stimulated brainweb database. By subjective evaluation neurologists and radiologists confirmed that the proposed method, VMD-TV shows prominent results in denoising Rician noise by preserving the anatomical features that are crucial for diagnosis [42]. D.Sreelakshmi et al. (2021) presented machine learning and deep learning based approaches that have been used to identify brain-related disorders. In this research, a CNN-ML based adaptive mean filter is designed for noise removal and brain-related disorder identification. This examination attains a better accuracy of 0.98, PSNR 56.02, positive rate of 0.95 [43]. Abhishek Sharma et al. (2021) proposed a denoising technique based on the advanced NLM method with Non-Subsampled Shearlet Transform (NSST). The proposed method is compared with state-of-the-art methods the study claims that various NLM-based techniques have some advantages and disadvantages, some are good for Rician noise, some are good for Gaussian noise and some fail to preserve fine and edge details of images. In proposed techniques, the NLM filter is modified to improve noise detection and noise removal quality, and NSST is used for better preservation of edges and fine details of images [44]. Mamta Juneja

Table 2
Summary of State-of-the-Art Denoising Approaches.

Authors	Year	Approach	Pros	Cons
S. Suryanarayana et al. [29]	2012	<ul style="list-style-type: none"> Developed filters and detection schemes for Gaussian noise Proposed method performs better than the standard mean filter 	<ul style="list-style-type: none"> Better edge preservation compared to standard mean filters 	<ul style="list-style-type: none"> Only good for Gaussian noise
Saritha Saladi et al. [30]	2017	<ul style="list-style-type: none"> Proposed spatially adaptive NLM filters which outperform conventional methods 	<ul style="list-style-type: none"> Preserve edges 	<ul style="list-style-type: none"> Computationally expensive
Worku Jifara et al. [31]	2017	<ul style="list-style-type: none"> Proposed a residual learning based approach 	<ul style="list-style-type: none"> Take less training time. 	<ul style="list-style-type: none"> Only tested for small datasets
S. Agarwal et al. [32]	2017	<ul style="list-style-type: none"> Compare wavelet-based thresholding techniques' efficiency 	<ul style="list-style-type: none"> Symlet transform shows the best performance 	<ul style="list-style-type: none"> Fine details are lost when there is a lot of noise
Ki Hwan Kim et al. [33]	2018	<ul style="list-style-type: none"> HR MR images are generated from downsampled MR images 	<ul style="list-style-type: none"> Ideal for accelerating routine MRI scanning 	<ul style="list-style-type: none"> Not good for smaller datasets
Shamima Nasrin et al. [34]	2019	<ul style="list-style-type: none"> Autoencoder based R2U-Net model is used 	<ul style="list-style-type: none"> Transfer learning between CT and MRI scans Reduce the computational cost less training time 	<ul style="list-style-type: none"> Requires more training for efficient performance
Xuexiao You et al. [35]	2019	<ul style="list-style-type: none"> An effective deep and wide CNN based approach is used for removing Rician-noise-perturbed images 	<ul style="list-style-type: none"> Computationally expensive 	
Hemalata V. Bhujle et al. [36]	2019	<ul style="list-style-type: none"> Studied various NLM based denoising techniques 	<ul style="list-style-type: none"> Shows good results in case of redundant images 	<ul style="list-style-type: none"> NLM based denoising is unable to preserve edges
Dibakar Sil et al. [37]	2019	<ul style="list-style-type: none"> Inception -v3 shows the best result for noise distribution in noisy images According to the paper if PSNR is below 30 dB, specific CNN will be valid for detecting noise distribution 	<ul style="list-style-type: none"> Able to preserve crucial details 	<ul style="list-style-type: none"> Unable to show much improvement in removing Gaussian noise
Dan Hong et al. [38]	2020	<ul style="list-style-type: none"> Proposed method FFA-DMRI 	<ul style="list-style-type: none"> Able to preserve sharp edges Can generate sharper images 	<ul style="list-style-type: none"> Only able to remove Rician noise efficiently
Bhawna Goyal et al. [39]	2020	<ul style="list-style-type: none"> Review of denoising methods 	<ul style="list-style-type: none"> Multi-resolution based algorithms work better than single-resolution ones 	<ul style="list-style-type: none"> Suggested to use a combination of various methods which can be computationally expensive
Miao Tian et al. [40]	2021	<ul style="list-style-type: none"> Proposed conditional GANs based approach for denoising 	<ul style="list-style-type: none"> Better denoising quality 	<ul style="list-style-type: none"> Not tested for other imaging techniques like CT and X-ray
S. Ramesh et al. [41]	2021	<ul style="list-style-type: none"> Proposed MLE-based KPCA for feature selection and for removing salt and pepper noise modified iterative groping median filter is proposed 	<ul style="list-style-type: none"> Prevent blur and preserve sharp edges Better feature selection 	<ul style="list-style-type: none"> High computational time
Divya Pankaj et al. [42]	2021	<ul style="list-style-type: none"> Proposed VMD-TV based on VMD for removing Rician noise 	<ul style="list-style-type: none"> VMD-TV is able to preserve anatomical features 	<ul style="list-style-type: none"> Works effectively only for Rician noise
D.Sreelakshmi et al. [43]	2021	<ul style="list-style-type: none"> CNN based mean filter is proposed for removing Rician noise 	<ul style="list-style-type: none"> Smooth out the image 	<ul style="list-style-type: none"> Unable to preserve edges
Abhishek Sharma et al. [44]	2021	<ul style="list-style-type: none"> Proposed advanced NLM method with NSST for denoising Modified NLM filter is good for noise detection and noise removal, NSST for the preservation of edges and fine details 	<ul style="list-style-type: none"> Higher denoising quality Able to reduce the blur Able to preserve the edges 	<ul style="list-style-type: none"> Not recommended in case of an excessive level of noise
Mamta Juneja et al. [45]	2021	<ul style="list-style-type: none"> A filtering-based technique, BSbFWT, and a deep learning approach, BBAuto-Net, are proposed 	<ul style="list-style-type: none"> Able to keep edges sharp Preserve anatomical details Reduces noise corruption It does not require the value of noise level 	<ul style="list-style-type: none"> BSbFWT performance is lacking in the case of larger datasets
Javier Gurrol-Ramos et al. [4]	2021	<ul style="list-style-type: none"> Proposed RDUNet 	<ul style="list-style-type: none"> Employed local residual learning to accelerate learning and prevent the vanishing gradient issue 	<ul style="list-style-type: none"> A distinct model must be trained for each type of noise

et al. (2021) proposed Bayes Shrinkage based Fused Wavelet Transform (BSbFWT) and Block based Autoencoder Network (BBAuto-Net) based on an autoencoder approach. These methods get around issues like suppressing the state-of-the-art visual details that are present. Additionally, it reduces noise corruption and improves anatomical detail, details to keep the edges sharp. Metrics score of BSbFWT are as follows PSNR (29.028), SSIM (0.747)and MSE (81.33) and for BBAuto-Net scores are PSNR (28.029), SSIM (0.581) and MSE (89.354) [45]. Javier Gurrol-Ramos et al. (2021) proposed RDUNet for denoising. The RDUNet's encoding and decoding layers are made up of densely connected convolutional layers that reuse feature maps and use local residual learning to avoid the vanishing gradient problem and accelerate the learning process. For comparison, the author employs additive Gaussian noise with values of 10, 30, and 50. In the case of grayscale images, the model obtained PSNR values of 34.39, 29.11, and 26.99, as well as SSIM values of 0.9297, 0.8193, and 0.7491. PSNR values for color images were 36.68, 31.43, and 29.12, with SSIM values of 0.9600, 0.8961, and 0.8465 [4].

The Table 2 represents the summary of various denoising approaches

and techniques over the past few years with their respective pros and cons.

4. Proposed methodology

The suggested BT-Autonet which is shown in the Fig. 2 is constructed with a series of convolutional layers, deconvolutional layers and a combination of additional layers to denoise the MRI contaminated by Gaussian, Rician and Rayleigh noise.

4.1. Bt-autonet model

The proposed BT-Autonet as shown in the Fig. 2 consists of a five block deep dense autoencoder with skip connections. The autoencoder is divided into two parts, the first is the encoding block, which employs convolution layers of varying strides. Second, the decoding part in which transpose convolutional layers are used along with the convolutional layers to upsample the reduced image coming from the encoding part of the autoencoder.

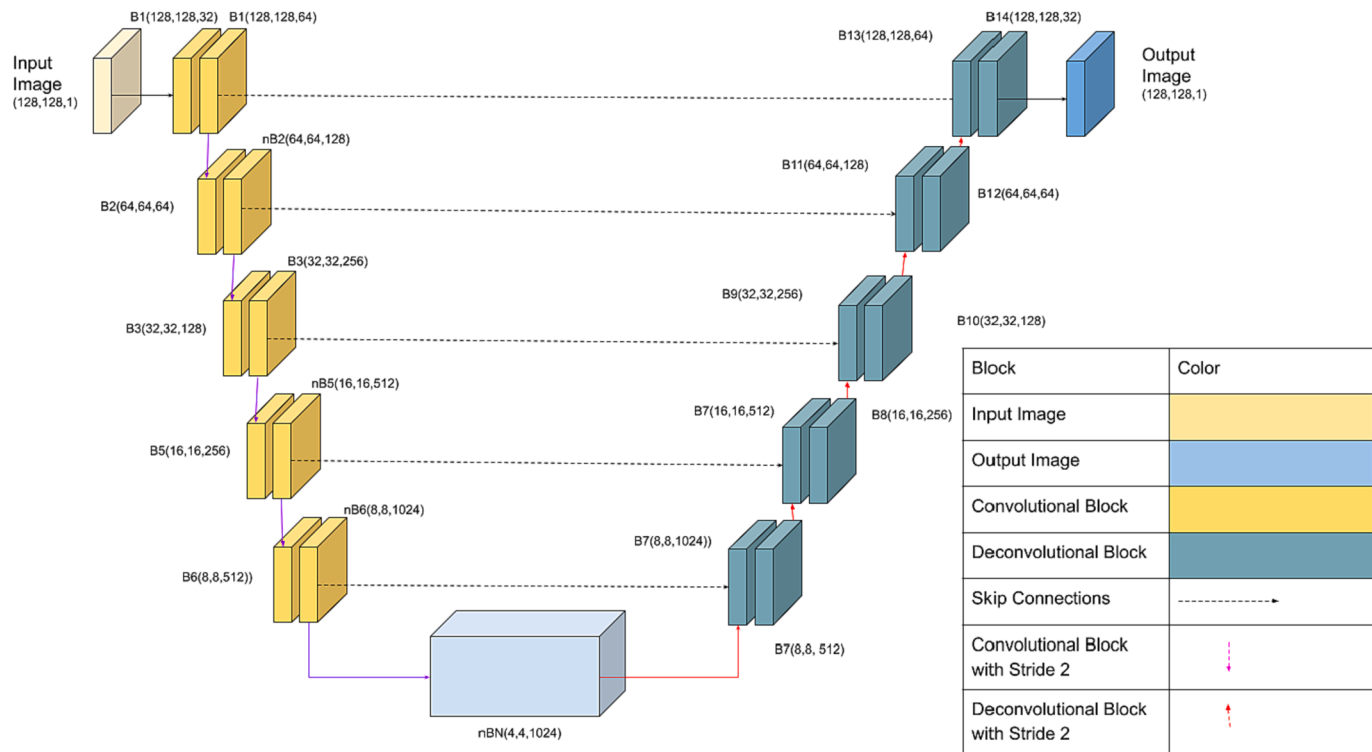


Fig. 2. Architecture of BT-Autonet Algorithm.

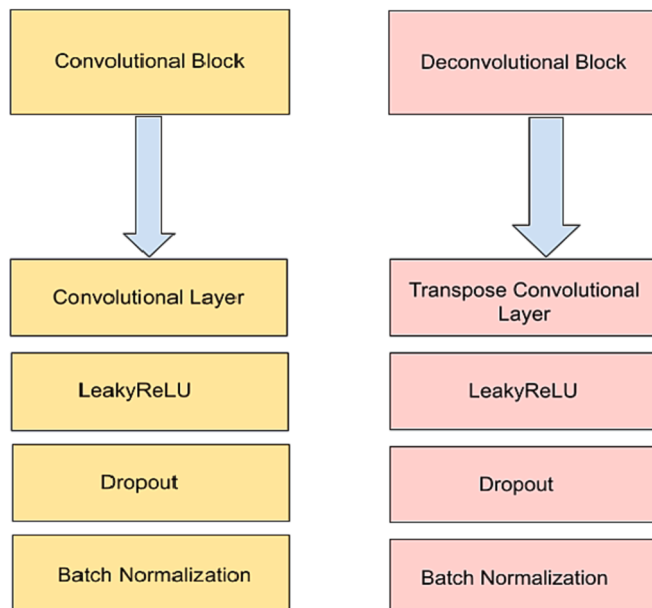


Fig. 3. Convolutional and Deconvolutional Block.

Fig. 2 depicts the model's layers and their dimensions. The encoding section gradually compresses the input image of size (128,128,1) to a bottleneck of dimension(4,4,1024). The encoder consists of convolutional blocks which are responsible for learning the features of the image. Every layer marked with n-suffix consists of the same convolutional block but with a stride of 2 which is used for downsampling. Their output is also added to the outputs of the layer of the decoding section using skip connections. Similar architecture is followed in the decoding block, n suffix blocks are used for upsampling with a deconvolutional block of stride 2 (convtranspose layer with stride 2). The image is

upsampled to the original size and skip connection output is added after every block. Moreover, instead of Rectified Linear Unit (ReLU) or Parametric Rectified Linear Unit (PReLU), Leaky Rectified Linear Unit (LeakyReLU) has been used as an activation function. Each activation output is fed to a dropout and batch normalization layer.

4.2. Convolutional layer

A convolutional layer is the main building block of a Convolutional Neural Network(CNN) which contains a set of filters(or kernels), parameters of which are to be learned throughout the training. Each filter interacts with the image to generate an activation map. Convolutional layers in BT-Autonet automatically learn a set of features from input images by using a large number of filters on the dataset as well as to downsample the image.

4.3. Transpose convolutional layer

Transpose convolutional layer is used to upsample the output using some learnable parameters so that the image can be reconstructed again. In BT-Autonet, transpose convolutional layers are used in decoding part of the network to upsample feature maps received from the subsequent layers resulting in an output denoised image of the original dimension.

4.4. Dropout layer

Dropout layers are usually applied after an application layer is applied to a convolutional layer. Dropout offers a very computationally cheap and remarkably effective regularization method to reduce overfitting and improve generalization error in deep neural networks of all kinds. In BT-Autonet, a dropout layer is used after the convolutional layer to drop some input values so that the model is more robust to noise, excels in losing noise data, and helps in better denoising.

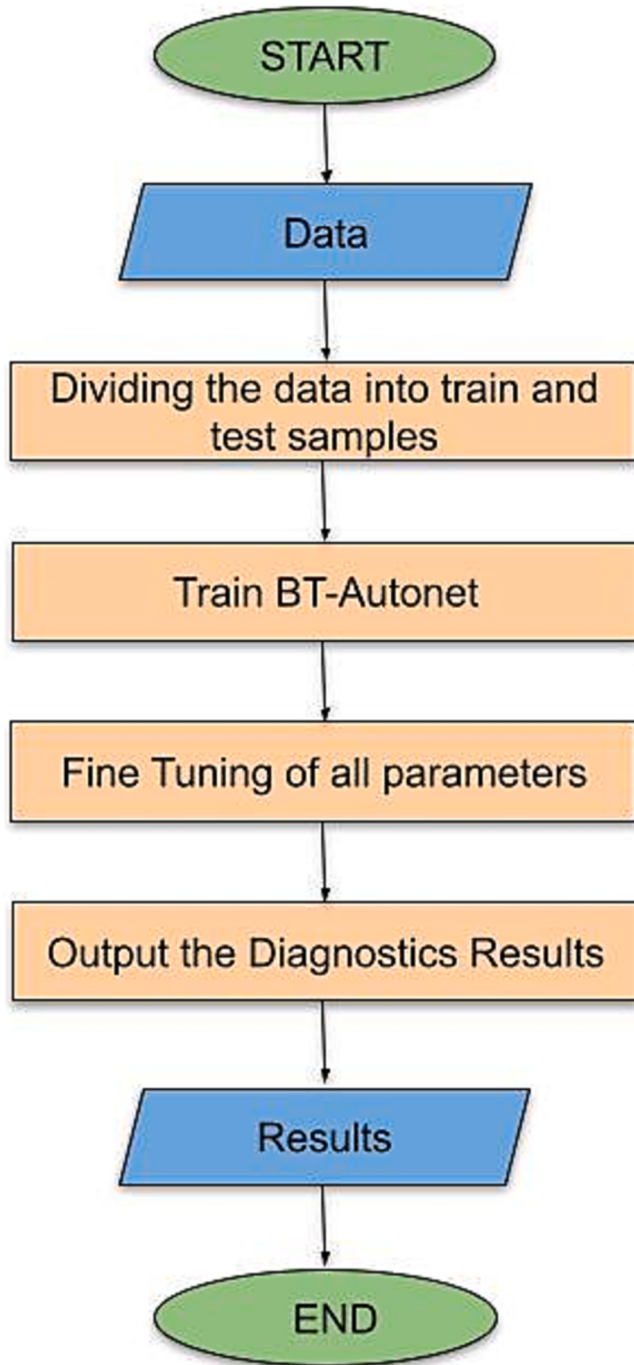


Fig. 4. Working of BT-Autonet.

4.5. Batch normalization layer

Batch normalization layers are also usually applied after the application layer is applied on convolutional layers. Batch normalization is a technique for training very deep neural networks that standardizes the inputs to a layer for each mini-batch which stabilizes the learning process and dramatically reduces the number of training epochs required to train deep networks. In BT-Autonet, batch normalization layers are used in the encoding part as well as the decoding part of the network to standardize the data.

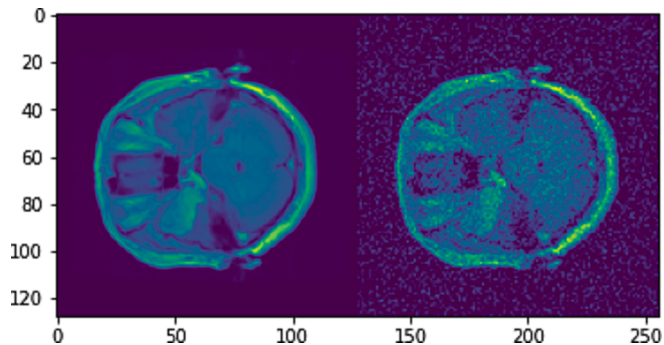


Fig. 5. Gaussian Noised Image.

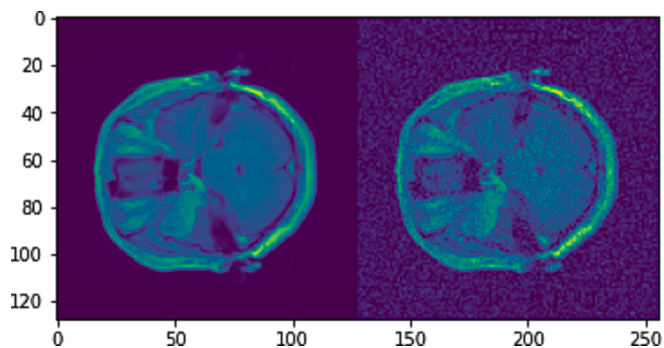


Fig. 6. Rician Noised Image.

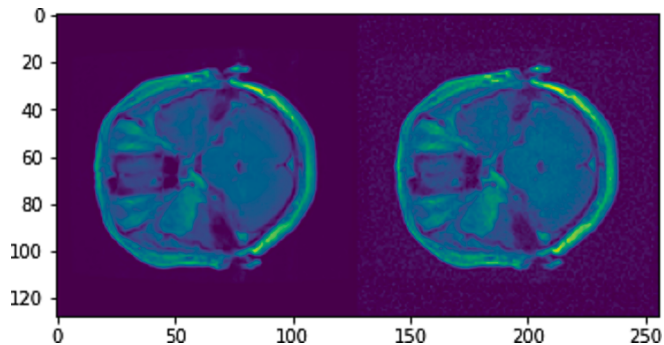


Fig. 7. Rayleigh Noised Image.

4.6. Convolutional block

The convolutional block consists of a convolutional layer with dimensions, kernel size, and stride varying depending on the layer. Followed by the convolutional block, the activation function used after each convolutional layer is LeakyReLU. The output from the activation function is fed to the dropout layer with a rate of 2 percent, which is then normalized by the batch normalization layer as shown in Fig. 3.

4.7. Deconvolutional block

The deconvolutional block consists of a transpose convolutional layer with dimensions, kernel size, and stride varying depending on the layer. Followed by the deconvolutional block, the activation function used after each deconvolutional layer is LeakyReLU. The output from the activation function is fed to the dropout layer with a rate of 2 percent which is then normalized by the batch normalization layer as shown in Fig. 3.

The Fig. 4 represents the working of BT-Autonet.

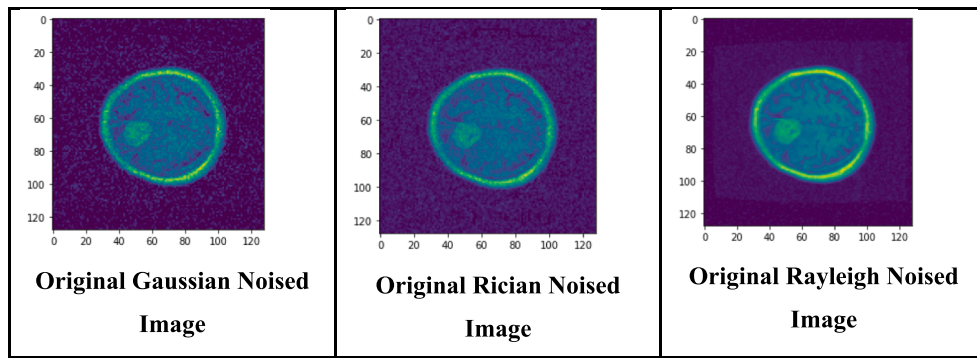


Fig. 8. Original Noised Images (128 × 128).

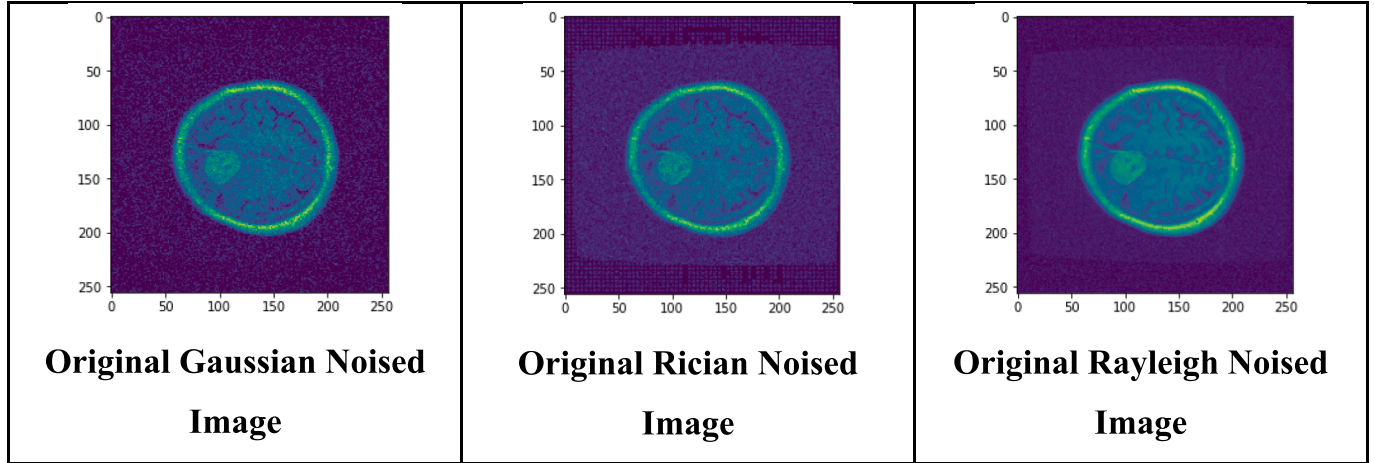


Fig. 9. Original Noised Images (256 × 256).

5. Results and discussion

This section describes the experimental setup and dataset, then compares the proposed classification network to the state-of-the-art solutions using standard performance criteria.

5.1. Experimental setup

The practical implementation was performed in python 3.9.0 using the scikit and skimage libraries. Tensorflow has been used for deep learning implementation of neural network models and efficient utilization of GPUs. The system has an Intel Xeon E5-2650 V4 CPU which has 48 cores with a peak operating frequency of 2.20 GHz and it has a memory of 256 gigabytes. The GPU hardware consists of the Nvidia RTX3090 which has 10496 Cuda cores with 24 GB VRAM, 384-bit bus width along with 1695 MHz maximum operating frequency.

5.2. Dataset description

The brain T1-weighted CE-MRI dataset was acquired from Nanfang Hospital, Guangzhou, China, and General Hospital, Tianjin Medical University, China, from 2005 to 2010. The dataset consists of 3064 slices from 233 patients, containing 708 meningiomas, 1426 gliomas, and 930 pituitary tumors. The images have an in-plane resolution of 512 × 512 with a pixel size of 0.49 × 0.49 mm². The other datasets such as the Gaussian, Rician, and Rayleigh noise dataset were made after applying various noise distributions on image dataset as mentioned below.

The Gaussian noised dataset consists of original dataset images with a Gaussian distribution applied to them with values of mean and sigma as 0 and 0.005 respectively. The Fig. 5 shows the original image on the

left and the Gaussian noised image on the right.

The Rician noised dataset comprises of the original image dataset images with Rician distribution applied on it with values of various parameters like base value, scale, and size being 5, 3, and 240 × 240 respectively. The Fig. 6 represents the original image on the left and the Rician noised image on the right.

The Rayleigh noised dataset is the original image dataset with Rayleigh distribution applied on it with values of random scale 5 and number of samples as 240 × 240 respectively. The Fig. 7 represents the original image on the left and the Rayleigh noised image on the right.

5.3. Performance metrics

There are several assessment indices available in the literature for validating denoising processes for quantitative evaluation. The effectiveness of the various filters and autoencoder based techniques presented in this study is evaluated using performance indicators such as MSE, PSNR, and SSIM.

5.3.1. Mean square error (MSE)

MSE is defined as the average square error, which is computed as the difference between the estimator and the estimated picture. It primarily refers to the predicted value of loss in the square because of randomness [46].

$$MSE = \frac{1}{m \times n} \sum_{i=0}^{m-1} \sum_{j=0}^{n-1} [I(x, y) - I'(x, y)]^2 \quad (5)$$

In Eq. (5) m × n are the dimensions of image, $I(x, y)$ is the initial image, $I'(x, y)$ is image after estimation. It always returns a positive value, and a lower value denotes better outcomes.

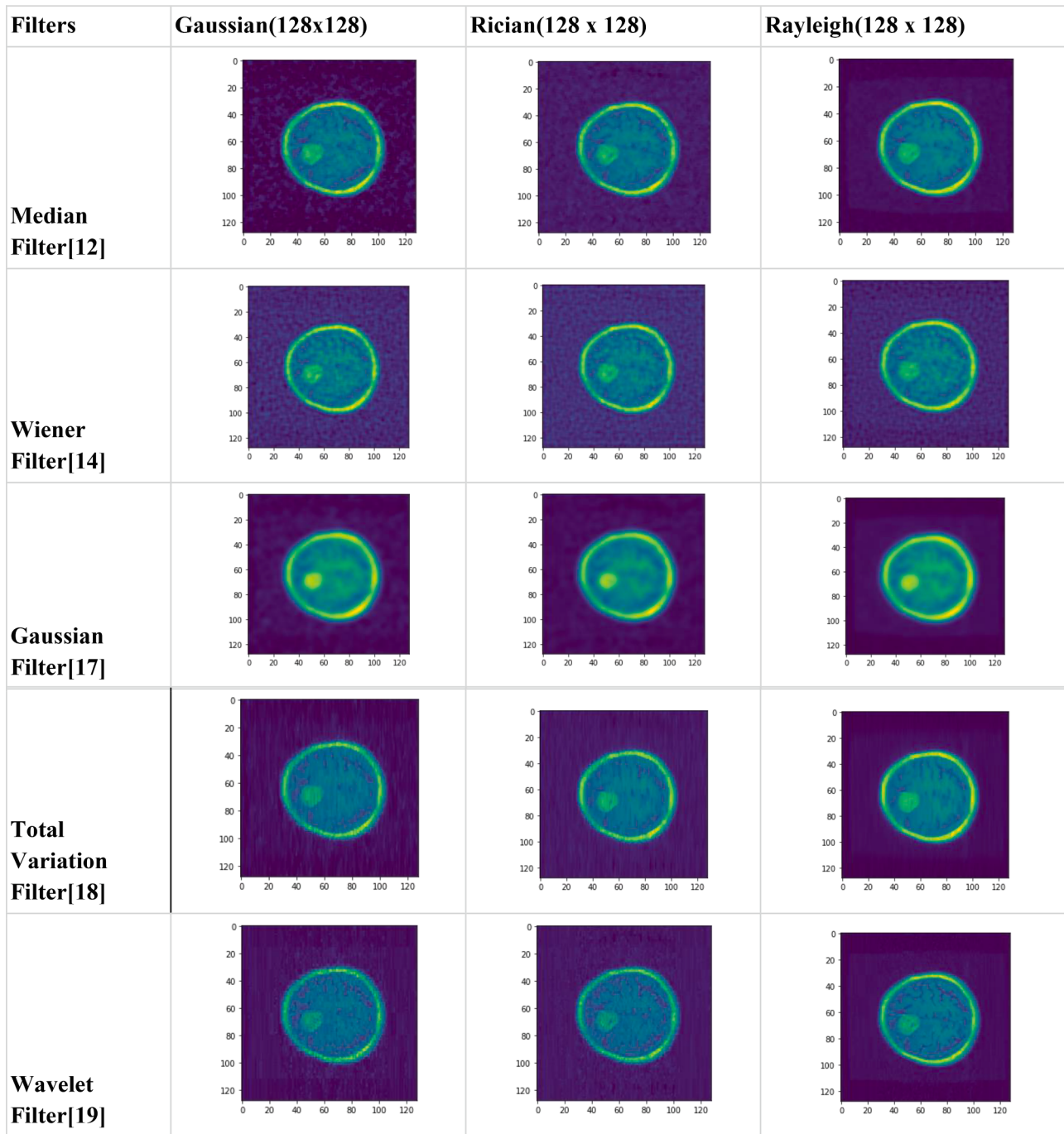


Fig. 10. Denoised Images of Gaussian Noise, Rician Noise and Rayleigh Noise of Size (128 × 128).

5.3.2. Peak signal-to-noise ratio (PSNR)

The PSNR is typically expressed as the ratio of the maximum signal value to the power of distortion noise that has an impact on the image's quality. The PSNR is expressed in terms of the logarithmic decibel scale because many images have a very wide dynamic range between the highest and smallest potential values of variable quantity [47].

It is defined as:

$$PSNR = 10 \log_{10} \left(\frac{MAX_i^2}{\sqrt{MSE}} \right) \quad (6)$$

Here in Eq. (6) MSE is the mean square error and MAX_i is the maximum value of pixels within the image. Higher value of PSNR

signifies better results.

5.3.3. Structure similarity index measure (SSIM)

SSIM measures how similar two images are to the original, altered image. It is used to rate the quality of an image. The degradation of the image is caused by a change in the structural information, which includes both luminance masking and contrast terms. Here, luminance refers to the deformity in the image that is typically harder to see in the brighter light. Contrast is the deformity that is obscured by abrupt changes and textured areas [48].

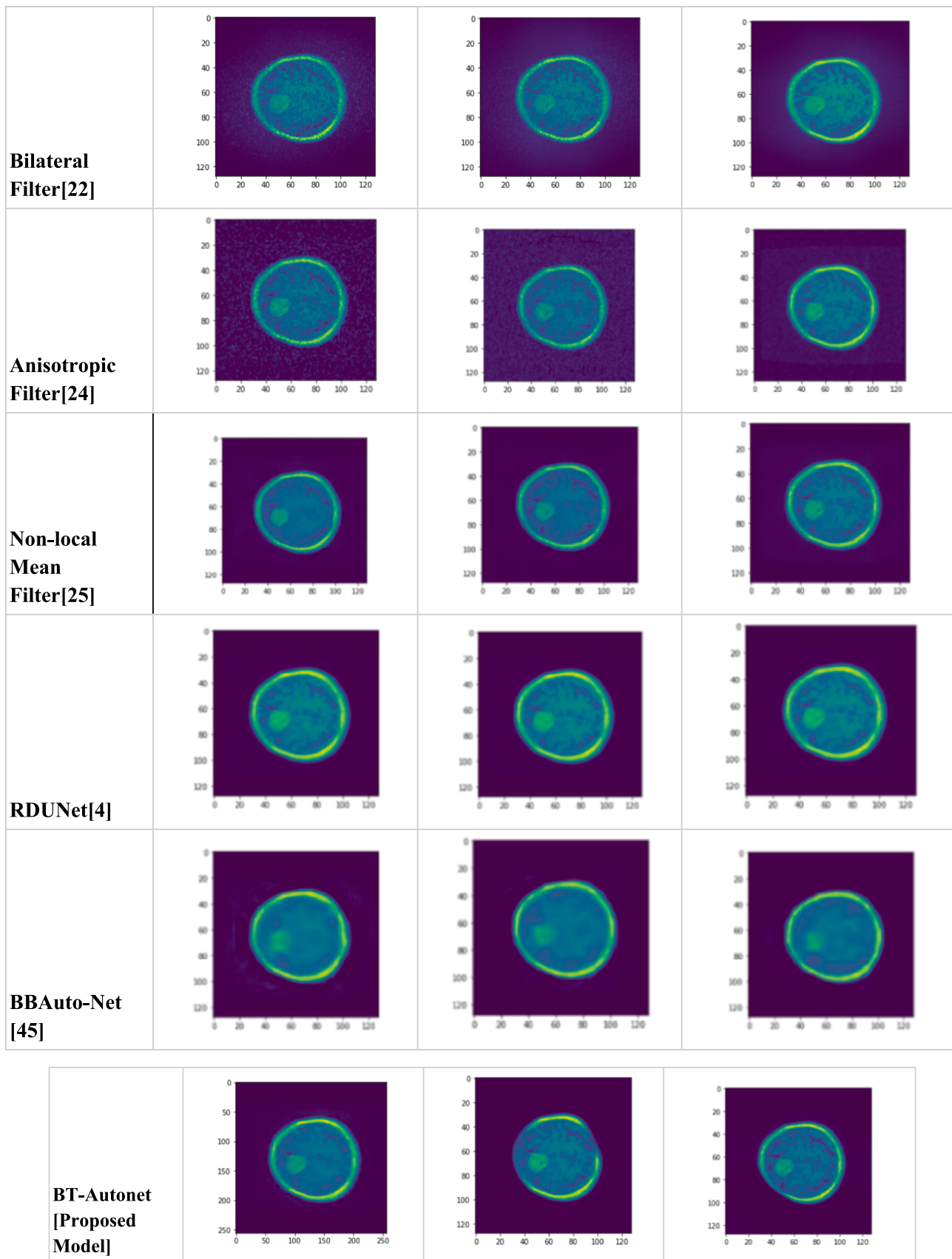


Fig. 10. (continued).

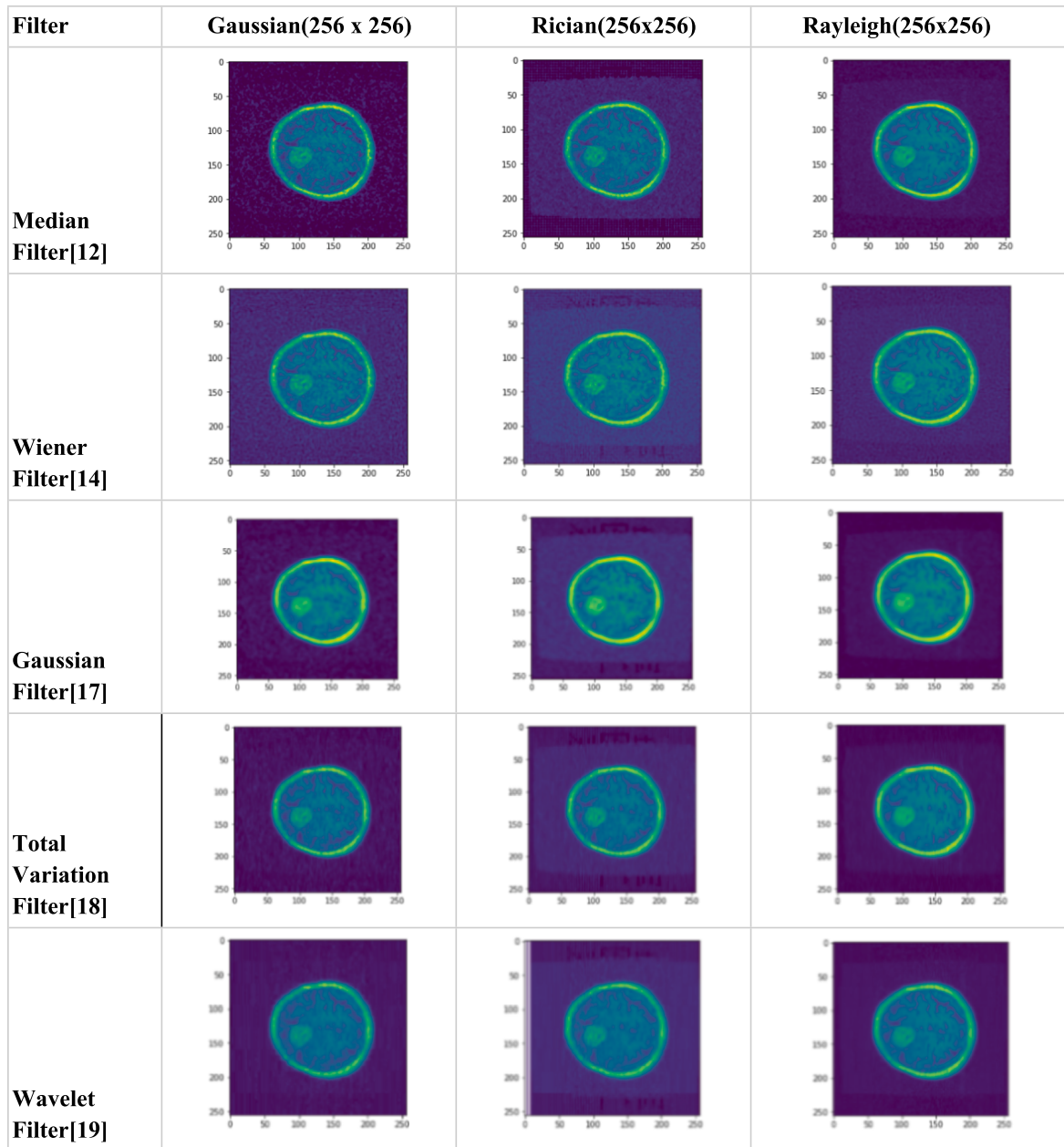


Fig. 11. Denoised Images of Gaussian Noise, Rician Noise and Rayleigh Noise of Size (256 × 256).

$$SSIM = \frac{(2\mu_F\mu_{F'} + c1)(2\sigma_{FF'} + c2)}{(\mu_F^2 + \mu_{F'}^2 + c1)(c_F^2 + \sigma_{F'}^2 + c2)} \quad (7)$$

In Eq. (7) $\sigma_F \wedge \sigma_{F'}$ are variance of F and F' , $c1 \wedge c2$ are variables to stabilize the division using weak denominator, $\mu_F \wedge \mu_{F'}$ are average of F and F' , while $F F'$ are input images. Higher values of SSIM signify better results.

5.4. Performance analysis

The following section contrasts the effectiveness of various denoising methods. For the comparative study two different sizes of noised images 128×128 and 256×256 were taken as shown in Figs. 8 and 9 respectively which are corrupted with Gaussian, Rician and Rayleigh noise.

5.4.1. Denoised Gaussian image

In this section various state-of-the-art filters, denoising methods, and BT-Autonet are used to remove Gaussian noise from MRI. For the comparative study, two different sizes of noised data were taken 128×128 and 256×256 , and the results of denoised images are shown in Figs. 10 and 11, respectively.

5.4.2. Denoised Rician image

In this section various state-of-the-art filters, denoising methods, and BT-Autonet are used to remove Rician noise from MRI. For the comparative study, two different sizes of noised data were taken 128×128 and 256×256 , and the results of denoised images are shown in the Figs. 10 and 11, respectively.

5.4.3. Denoised Rayleigh image

In this section various state-of-the-art filters, denoising methods, and

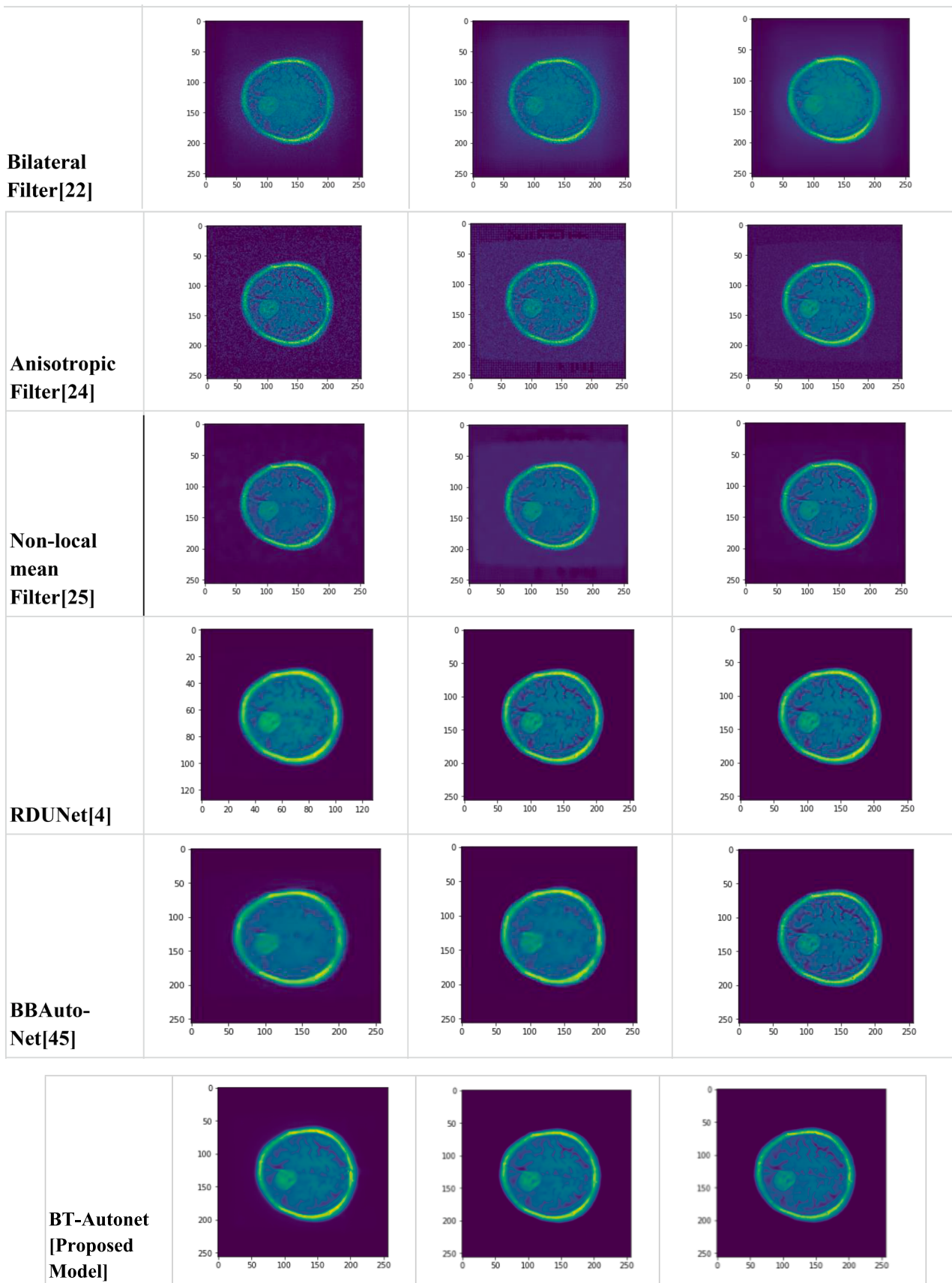


Fig. 11. (continued).

Table 3

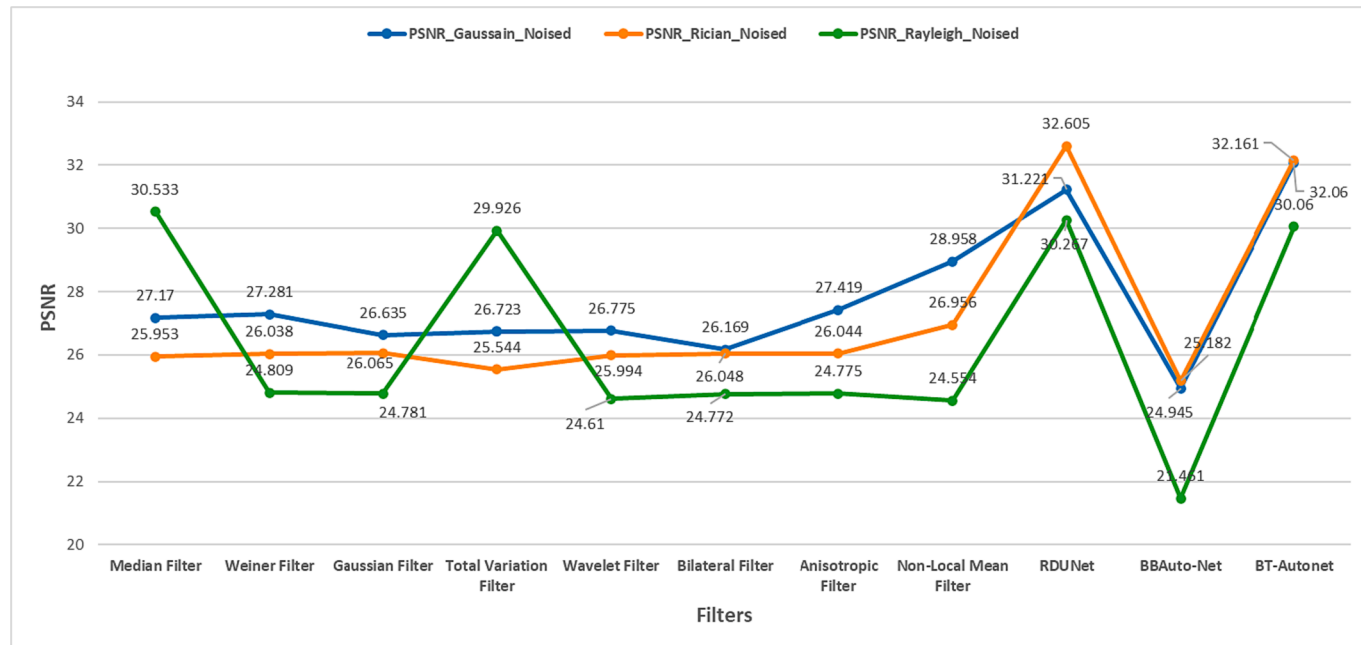
Comparative Study of Proposed Model with Existing Approaches.

Dataset Size:(3064,128,128,1)

Filters	Gaussian Dataset(mean = 0, var = 0.005)			Rician Dataset(variances =(0.05,0.05))			Rayleigh DatasetRayleigh dataset (scale = 5)		
	PSNR	SSIM	MSE	PSNR	SSIM	MSE	PSNR	SSIM	MSE
Median Filter[12]	27.17	0.855	45.396	25.953	0.79	66.643	30.533	0.929	82.475
Wiener Filter[14]	27.281	0.817	54.802	26.038	0.778	66.152	24.809	0.861	94.694
Gaussian Filter[17]	26.635	0.837	51.246	26.065	0.779	66.463	24.781	0.867	92.112
Total Variation Filter[18]	26.723	0.808	55.561	25.544	0.773	73.859	29.926	0.917	86.672
Wavelet Filter[19]	26.775	0.812	54.348	25.994	0.779	71.888	24.61	0.858	92.637
Bilateral Filter[22]	26.169	0.803	50.315	26.048	0.768	70.877	24.772	0.86	83.951
Anisotropic Filter[24]				26.044	0.793	67.686	24.775	0.862	94.484
Non-Local Mean Filter[25]	28.958	0.863	41.929	26.956	0.81	72.521	24.554	0.849	92.57
RDUNet[4]	31.221	0.825	29.145	32.605	0.822	19.951	30.267	0.739	42.674
BBAuto-Net [45]	24.945	0.791	47.712	25.182	0.779	45.033	21.461	0.73	60.373
BT-Autonet[Proposed]	32.06	0.939	25.179	32.161	0.942	23.129	30.06	0.962	44.378

Dataset Size:(3064,256,256,1)

Filters	Gaussian Dataset (mean = 0, var = 0.01)			Rician Dataset (variances =(0.01,0.1))			Rayleigh Dataset (scale = 10)		
	PSNR	SSIM	MSE	PSNR	SSIM	MSE	PSNR	SSIM	MSE
Median Filter[12]	27.277	0.778	53.597	23.98	0.674	73.745	26.041	0.772	108.371
Wiener Filter[14]	25.74	0.669	71.582	23.324	0.638	78.082	25.703	0.757	103.403
Gaussian Filter[17]	27.695	0.767	65.595	23.813	0.696	73.38	25.476	0.763	117.926
Total Variation Filter[18]	26.204	0.705	71.195	23.397	0.659	76.634	25.253	0.745	115.541
Wavelet Filter[19]	26.544	0.737	71.028	23.178	0.667	77.305	25.646	0.762	114.325
Bilateral Filter[22]	24.287	0.625	64.57	23.172	0.614	79.731	25.787	0.76	107.495
Anisotropic Filter[24]			65.596	23.803	0.685	73.79	25.655	0.768	115.27
Non-Local Mean Filter[25]	28.463	0.788	61.868	24.084	0.7	73.925	26.059	0.778	124.392
RDUNet [4]	28.612	0.625	51.608	29.187	0.708	40.017	26.203	0.875	50.746
BBAuto-Net[45]	26.865	0.797	50.42	26.166	0.83	54.426	26.240	0.735	53.944
BT-Autonet[Proposed]	30.91	0.935	30.036	32.84	0.93	41.684	31.676	0.967	45.219

**Fig. 12.** Comparative Analysis of PSNR Value of Proposed Model with Existing Approaches for Size(128 × 128).

BT-Autonet are used to remove Rayleigh noise from MRI. For the comparative study, two different sizes of noised data were taken 128 × 128 and 256 × 256, and the results of denoised images are shown in the Figs. 10 and 11, respectively.

6. Discussion

MRI, which is the common modality used for the diagnosis of brain tumors, is prone to a certain amount of Gaussian, Rician and Rayleigh noise. Filters used till date remove the noise at the verge of over-

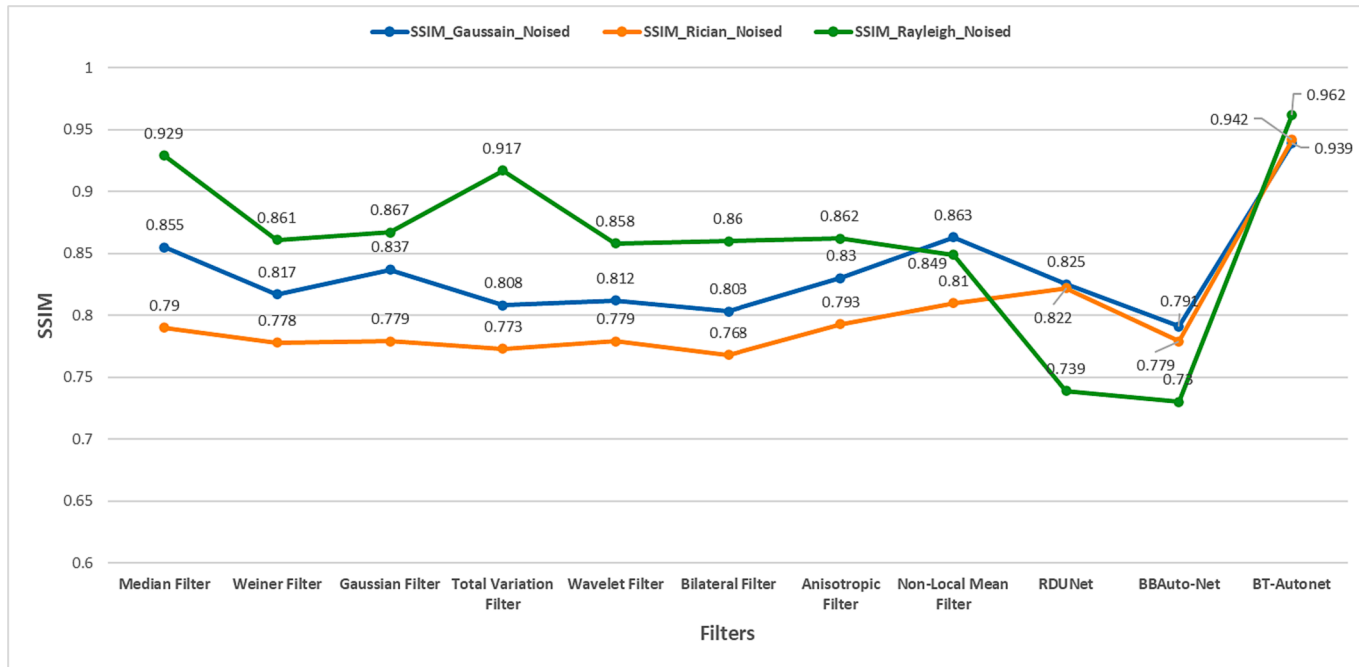


Fig. 13. Comparative Analysis of SSIM Value of Proposed Model with Existing Approaches for Size (128 × 128).

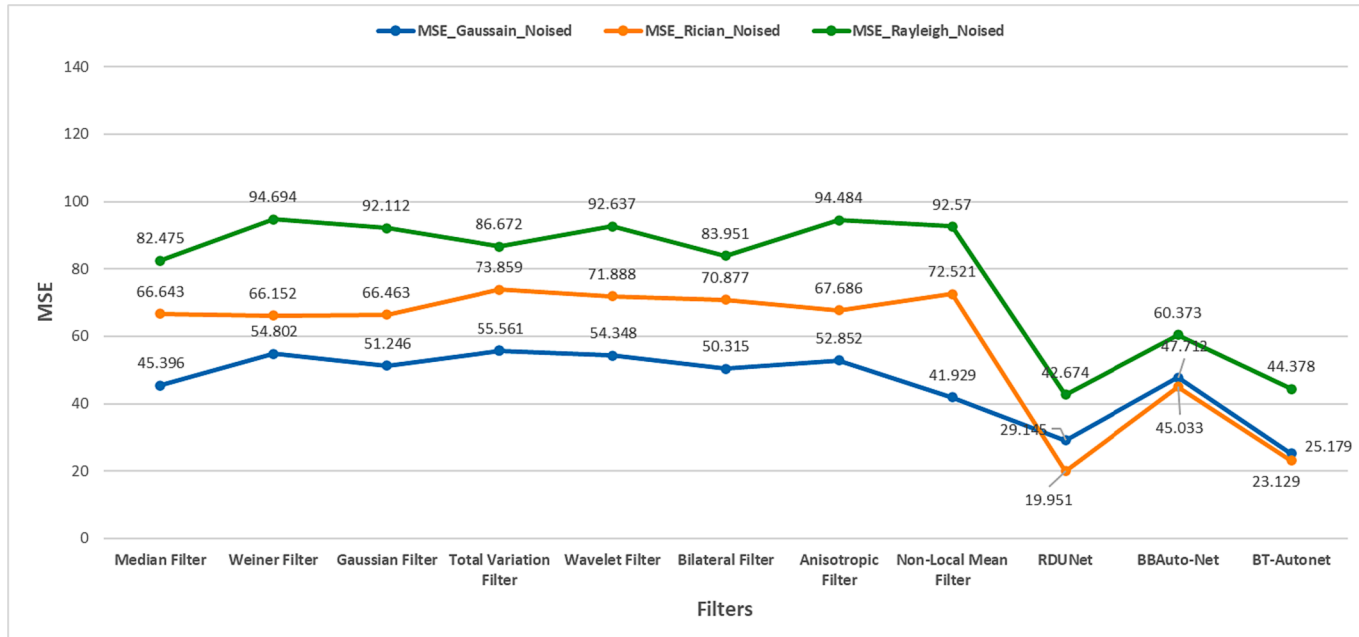


Fig. 14. Comparative Analysis of MSE value of Proposed Model with Existing Approaches for Size (128 × 128).

smoothing the image, leading to the loss of significant edge details. Thus, a deep convolutional autoencoder approach has been presented in this study to resolve the issues in the state-of-the-art. The deep learning approach provided more defining results in comparison to the traditional approaches. Also, for a larger dataset, autoencoder based deep learning gave more accuracy and it considered the hidden features in addition to the preservation of the features during the computation process while predicting the outputs of the denoised images. Further, on the basis of experimental analysis different observations have been made such as, the filter with high error reflects low quality image and hence, lower value of PSNR. Whereas, less error gives better image quality with a higher value of PSNR. Further, Table 3 presents the results

of metrics such as PSNR, MSE and SSIM obtained after applying various classical filters and autoencoders, including with the proposed network BT-Autonet.

The Fig. 12 represents the value of PSNR for different filters with respect to Gaussian, Rician and Rayleigh noised datasets of 128 × 128 size images. As shown in the figure, BT-Autonet has the best score out of all the denoising techniques applied on the Gaussian noised dataset with a value of 32.06. RDUNet has the best score out of all the denoising techniques applied on the Rician noised dataset with a value of 32.605. Median filter has the best score out of all the denoising techniques applied on the Rayleigh noised dataset with a value 30.533.

The Fig. 13 represents the value of SSIM for different filters with

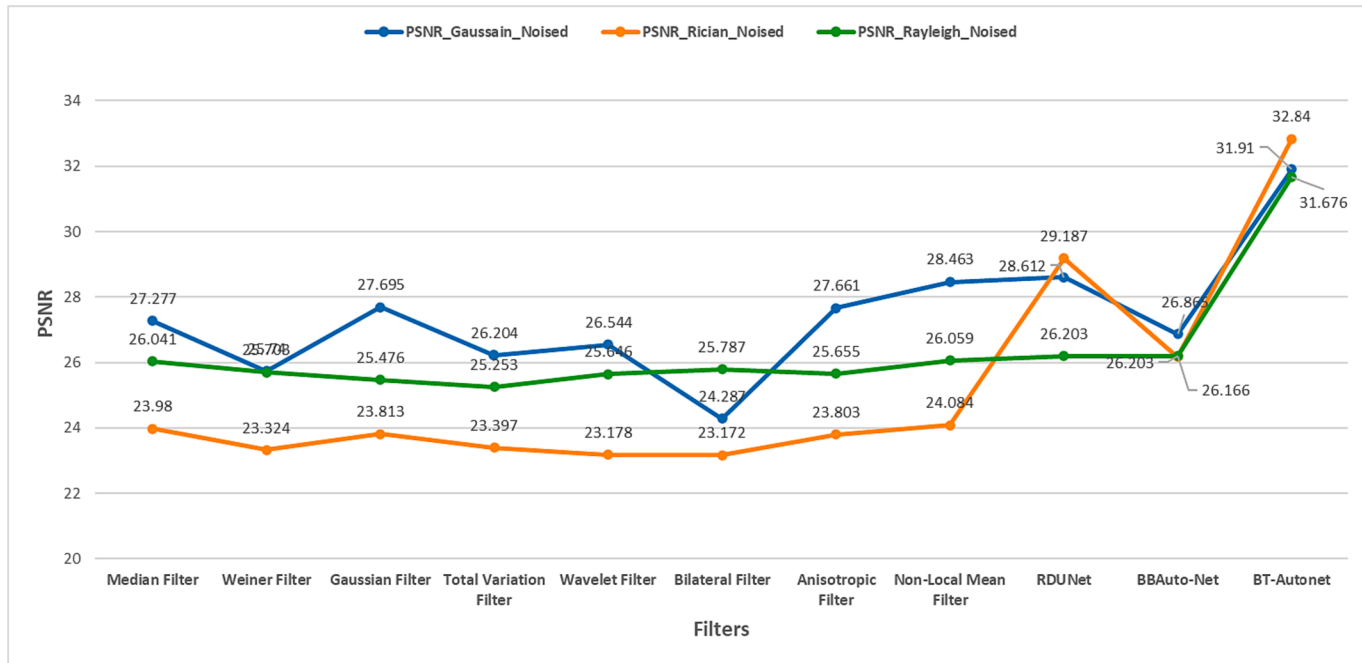


Fig. 15. Comparative Analysis of PSNR Value of Proposed Model with Existing Approaches for Size (256 × 256).

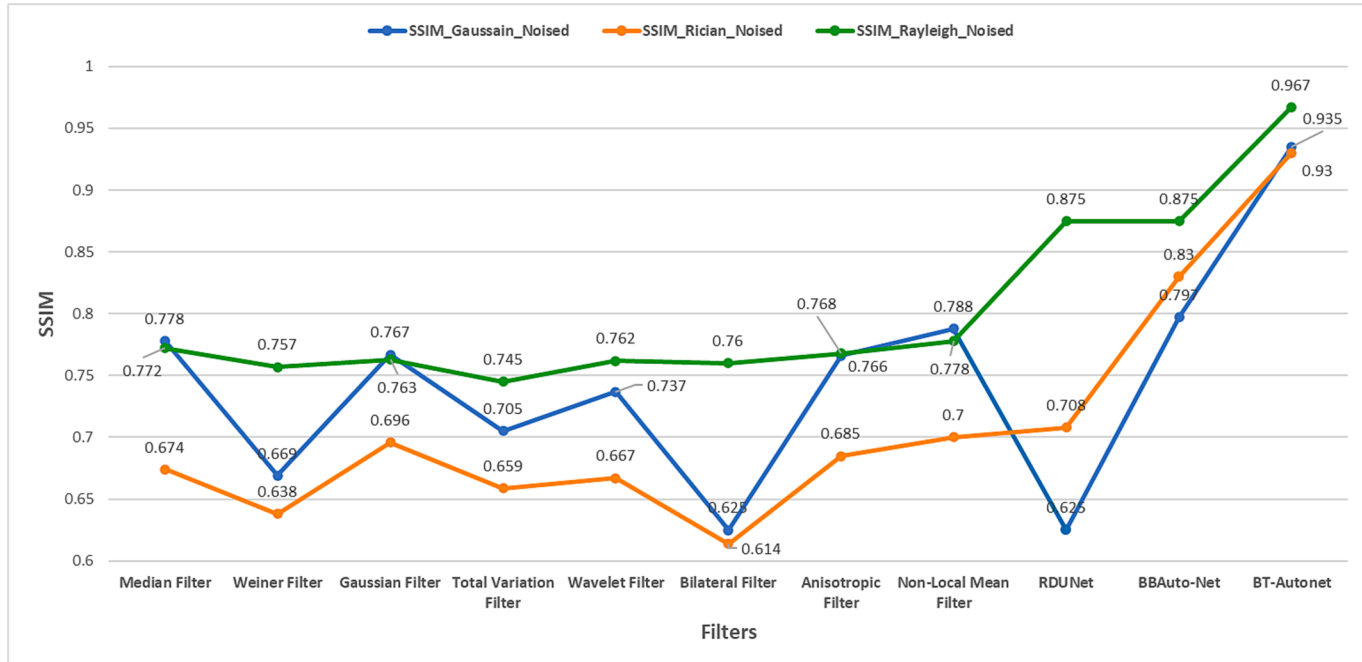


Fig. 16. Comparative Analysis of SSIM Value of Proposed Model with Existing Approaches for Size (256 × 256).

respect to Gaussian, Rician and Rayleigh noised datasets of 128×128 size images. The plot depicts that BT-Autonet has the best score out of all the denoising techniques applied on the Gaussian, Rician and Rayleigh noised datasets with values 0.939, 0.942 and 0.962 respectively.

The Fig. 14 depicts the value of MSE for different filters with respect to Gaussian, Rician and Rayleigh noised datasets of 128×128 size images. As shown in the Fig. 14, the BT-Autonet has the best score out of all the denoising techniques applied on the Gaussian noised dataset with a value of 25.179. RDUNet has the best score out of all the denoising techniques applied on the Rician noised and Rayleigh noised datasets with values 19.951 and 42.674 respectively.

The Fig. 15 represents the value of PSNR for different filters with respect to Gaussian, Rician and Rayleigh noised datasets of 256×256 size images. As shown in the Fig. 15, BT-Autonet has the best score out of all the denoising techniques applied on the Gaussian noised, Rician noised and Rayleigh noised with the value of 31.91, 32.84 and 31.676 respectively.

The Fig. 16 represents the value of SSIM for different filters applied on Gaussian, Rician and Rayleigh noised datasets of 256×256 size images. As shown in the Fig. 16, BT-Autonet has the best score out of all the denoising techniques applied on the Gaussian noised, Rician noised and Rayleigh noised with the value of 0.935, 0.93 and 0.967

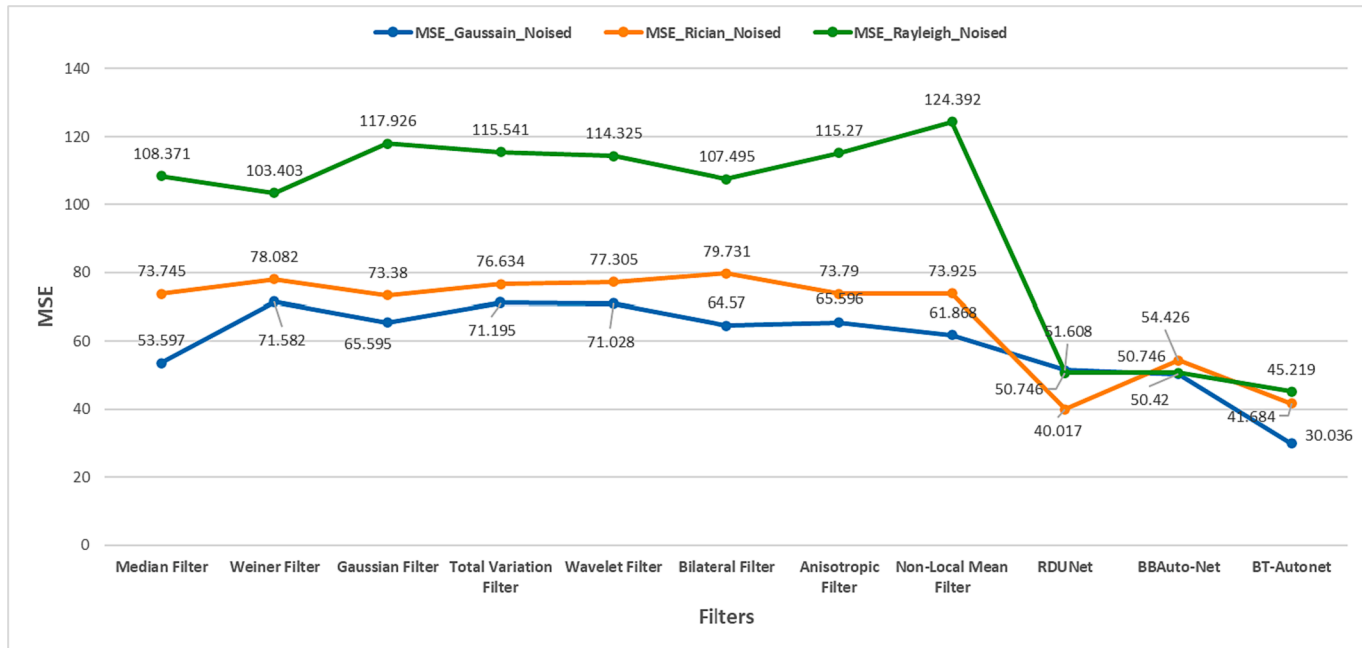


Fig. 17. Comparative Analysis of MSE Value of Proposed Model with Existing Approaches for Size (256 × 256).

Table 4

Comparison of the Execution Time of Proposed Model with Existing Approaches.

S. No.	Filters	(128 × 128)			(256 × 256)		
		Denoised Gaussian Image (Execution time in seconds)	Denoised Rician Image (Execution time in seconds)	Denoised Rayleigh Image (Execution time in seconds)	Denoised Gaussian Image (Execution time in seconds)	Denoised Rician Image (Execution time in seconds)	Denoised Rayleigh Image (Execution time in seconds)
1.	Median Filter[12]	0.006	0.006	0.006	0.010	0.010	0.02
2.	Wiener Filter[14]	0.006	0.048	0.048	0.126	0.125	0.121
3.	Gaussian Filter[17]	0.004	0.005	0.005	0.014	0.014	0.014
4.	Total Variation Filter[18]	0.120	0.123	0.104	0.260	0.312	0.286
5.	Wavelet Filter[19]	0.009	0.008	0.008	0.018	0.019	0.017
6.	Bilateral Filter[22]	0.027	0.0271	0.028	0.105	0.103	0.105
7.	Anisotropic Filter [24]	0.0054	0.0058	0.0056	0.006	0.017	0.005
8.	Non-local Mean Filter[25]	0.031	0.03	0.029	0.123	0.133	0.121
9.	RDUNet [4]	557	611	582	528	606	608
10.	BBAuto-Net[45]	2	2.5	2	1	2	2.5
11.	BT-Autonet [Proposed]	10.5	11	11	25	27	26

respectively.

The Fig. 17 depicts the value of MSE for different filters applied on Gaussian, Rician and Rayleigh noised datasets of 256 × 256 size images. As shown in the Fig. 17, BT-Autonet has the best score out of all the denoising techniques applied on the Gaussian noised and Rayleigh noised dataset with the value of 30.036 and 45.219 respectively. The RDUNet has the best score out of all the denoising techniques applied on the Rician noised dataset with the value of 40.017.

By the analysis of various state-of-the-art filters and denoising methods, for the Gaussian noised dataset (128 × 128), BT-Autonet shows the best result out of all the denoising techniques with the highest PSNR, SSIM, and MSE values of 32.06, 0.939 and 25.179 respectively, and for the Gaussian noised dataset (256 × 256), BT-Autonet shows the best result out of all the denoising techniques, with the highest PSNR, SSIM, and MSE values of 31.91, 0.935 and 30.036 respectively. For the Rician noised dataset (128 × 128), RDUNet shows the highest PSNR value of 32.605 but the proposed method shows the

best SSIM value of 0.94 and shows comparatively reasonable PSNR and MSE values and, for the Rician noised dataset (256 × 256) proposed method BT-Autonet shows the best score out of all the filters and denoising methods with the highest PSNR and SSIM values of 32.84 and 0.93 respectively, and second lowest value of MSE with a minute margin. For the Rayleigh noised dataset (128 × 128) median filter shows the highest PSNR score of 30.533 but a very high MSE score of 82.475 compared to which proposed method has the overall best balanced out metrics out of all the methods, with a good PSNR score of 30.06 and shows one the best SSIM and MSE score of 0.962 and 44.738 respectively, for Rayleigh noised dataset (256 × 256) The proposed model shows the best PSNR value of 31.676, the best SSIM value of 0.967, and the lowest MSE value of 45.219.

The Table 4 presents the execution time(in seconds) taken by the filters as well as the autoencoders based approaches for the denoising of Gaussian, Rician and Rayleigh noise.

Although various filters like Median, Wiener, Gaussian and other

Table 5

Parameters Used in Considered Approaches.

S. no.	Filters	Number of parameters
1.	Median Filter[12]	Central value of the image matrix is replaced by the median of all pixel values by taking window size N = 3.
2.	Wiener Filter[14]	Kernel size = (5,5) is used in the filter.
3.	Gaussian Filter[17]	$\sigma = 2$ is used in the filter.
4.	Total Variation Filter[18]	Weight = 0.1 is used in the filter (denoise_tv_chambolle).
5.	Wavelet Filter[19]	rescale_sigma = True is used in the filter.
6.	Bilateral Filter[22]	$\sigma_{spatial} = 15$ is used in the filter.
7.	Anisotropic Filter [24]	Iteration = 5, conduction coefficient kappa = 50, speed of diffusion gamma = 0.0057 and option = 1 is used in the filter.
8.	Non-local Mean Filter[25]	Patch size = 5, patch distance = 6 and fat_mode = True is used in the filter.
9.	RDUNet[4]	The deep neural network consists of 125 layers consisting of convolutional layer(64), add(59), transpose convolutional(2), Batch size = 16, epochs = 100, optimizer = adam and activation function = PReLU is used in the model
10.	BBAuto-Net[45]	The neural network includes 14 layers consisting of convolutional(7), max pooling(3), upsampling(3), and dropout(1). Batch size = 10, epochs = 100, optimizer = adam and activation function = ReLU is used in the model.
11.	BT-Autonet [Proposed Model]	The deep neural network includes 21 blocks consisting of convolutional blocks(16) and deconvolutional blocks(5) which contain convolutional(16), dropout(21), batch normalization (21), transpose convolutional(5), batch size = 64, epochs 100, optimizer = adam and activation function = LeakyReLU is used in the model

filters have fairly less conversion time than our proposed model, there are also a lot of problems associated with these such as the retention of edge features, blotting of images and information loss due to compression. Moreover, the existing BBAuto-Net is a light autoencoder which also suffers from the problem of feature retention due to the small number of convolutional layers. As such only RDUNet compares to the category of our proposed model and the proposed model BT-Autonet outperforms it in terms of conversion time as well as accuracy metrics with the conversion time of 11 s for 128×128 dataset and 27 s for 256×256 dataset.

Furthermore, Table 5 discusses the parameters employed in filters and autoencoder based approaches.

7. Conclusion and future scope

The presence of noise in MRI is detrimental to its quality and compromised image quality is a hindrance for an effective feature extraction, analysis, quantitative measurements and recognition of tumor from medical images. Denoising of an image is considered as a vital preprocessing and essential step and for enabling a meaningful analysis of the acquired images. A properly denoised image also helps in attaining better results during segmentation and classification. Hence, it has a significant impact on the effectiveness of CAD systems. To remove the noise from MRI more effectively and efficiently, BT-Autonet has been proposed along with an in-depth comparison of various MRI denoising techniques. In terms of accuracy metrics, proposed model (BT-Autonet) clearly outperforms other filters and denoising techniques, although RDUNet falls into the category of the proposed model but BT-Autonet has an edge due to its less complexity and light autoencoder properties over RDUNet, which in turn improve execution time and accuracy on major testing scenarios. The BT-Autonet model aims to preserve the quality of the images after denoising, which may help in achieving better results during the detection or segmentation of the tumor. BT-Autonet would significantly advance the field of medical

diagnosis and aid physicians in the analysis of MRI by providing superiorly denoised images. In future, it is proposed to eliminate other noises while improving the overall accuracy of this model. Additionally, a concerted effort will be made to speed up execution time and substantially enhance the values of performance metrics, mainly the PSNR, SSIM, and MSE for images with higher resolutions.

CRediT authorship contribution statement

Mamta Juneja: Conceptualization, Methodology, Project administration, Supervision, Software. **Ashwani Rathee:** Methodology, Data acquisition, Formal analysis, Visualization. **Rishabh Verma:** Results Analysis, Formal analysis, Methodology, Data Validation. **Raag Bhutani:** Data Acquisition, Methodology, Formal analysis, Visualization. **Shashank Baghel:** Investigation, Writing – original draft, Writing – review & editing. **Sumindar Kaur Saini:** Writing – review & editing. **Prashant Jindal:** Conceptualization, Results Validation, Project Funding, Project administration, Resources.

Declaration of Competing Interest

The authors declare that they have no known competing financial interests or personal relationships that could have appeared to influence the work reported in this paper.

Data availability

Data will be made available on request.

Acknowledgments

The authors are grateful to the Ministry of Human Resource Development (MHRD), Govt. of India for funding this project(17-11/2015-PN-1) under Design Innovation Centre(DIC) sub-theme Medical Devices and Restorative Technologies, UIET, Panjab University, Chandigarh.

Funding: This project was funded by the Ministry of Human Resource Development (MHRD), Government of India with grant number(17-11/2015-PN-1).

References

- [1] M. Juneja, S.K. Saini, J. Gupta, P. Garg, N. Thakur, A. Sharma, M. Mehta, P. Jindal, Survey of denoising, segmentation and classification of magnetic resonance imaging for prostate cancer, *Multimed. Tools Appl.* 80 (19) (2021 Aug) 29199–29249.
- [2] G. Garg, M. Juneja, A survey of denoising techniques for multi-parametric prostate MRI, *Multimed. Tools Appl.* 78 (10) (2019 May) 12689–12722.
- [3] Mamta Juneja, Kaur Saini, Sumindar, Sambhav Kaul, Rajarshi Acharyya, Niharika Thakur, Prashant Jindal, Denoising of magnetic resonance imaging using Bayes shrinkage-based fused wavelet transform and autoencoder based deep learning approach, *Biomed. Signal Process. Control* 69 (2021) 102844. 10.1016/j.bspc.2021.102844.
- [4] J. Girola-Ramos, O. Dalmau, T.E. Alarcón, A residual dense U-Net neural network for image denoising, *IEEE Access* 22 (9) (2021 Feb) 31742–31754.
- [5] A. Macovski, Noise in MRI, *Magn. Reson. Med.* 36 (3) (1996 Sep) 494–497.
- [6] H. Gudbjartsson, S. Patz, The Rician distribution of noisy MRI data, *Magn. Reson. Med.* 34 (6) (1995 Dec) 910–914.
- [7] J. Elterman, B. Goossens, A. Pizurica, W. Philips, Removal of correlated Rician noise in magnetic resonance imaging, in: 2008 16th European Signal Processing Conference, 2008 Aug 25, pp. 1–5. IEEE.
- [8] P. Singh, R. Shree, A comparative study to noise models and image restoration techniques, *International Journal of Computer Applications*. 149 (1) (2016 Sep) 18–27.
- [9] Ali HM. A new method to remove salt & pepper noise in Magnetic Resonance Images, in: 2016 11th International Conference on Computer Engineering & Systems (ICCES), 2016 Dec 20, pp. 155–160. IEEE.
- [10] B. Goyal, S. Agrawal, B.S. Sohi, Noise issues prevailing in various types of medical images, *Biomed. Pharmacol. J.* 11 (3) (2018) 1227.
- [11] G. Devarajan, V.K. Aatre, C.S. Sridhar, Analysis of median filter, in: ACE '90. Proceedings of [XVI Annual Convention and Exhibition of the IEEE In India], 1990, pp. 274–276, 10.1109/ACE.1990.762694. <https://ieeexplore.ieee.org/document/762694>.

- [12] M.K. Abd-Ellah, A.I. Awad, A.A. Khalaf, H.F. Hamed, Design and implementation of a computer-aided diagnosis system for brain tumor classification, in: 2016 28th International Conference on Microelectronics(ICM) 2016 Dec 17, pp. 73–76. IEEE.
- [13] B.A. Mohammed, M.S. Al-Ani, An efficient approach to diagnose brain tumors through deep CNN, *Math. Biosci. Eng.* 1 (18) (2020 Dec) 851–867.
- [14] S. Anitha, L. Kola, P. Sushma, S. Archana, Analysis of filtering and novel technique for noise removal in MRI and CT images, in: 2017 International Conference on Electrical, Electronics, Communication, Computer, and Optimization Techniques (ICEECCOT), 2017 Dec 15, pp. 1–3. IEEE.
- [15] H. Naimi, A.B. Adamou-Mitiche, L. Mitiche, Medical image denoising using dual tree complex thresholding wavelet transform and Wiener filter, *J. King Saud Univ.-Comput. Inform. Sci.* 27 (1) (2015 Jan 1) 40–45.
- [16] M. Mittal, L.M. Goyal, S. Kaur, I. Kaur, D. Jude Hemanth, Deep learning based enhanced tumor segmentation approach for MR brain images, *Appl. Soft Comput.* 78 (2019) 346–354.
- [17] T. Hossain, F.S. Shishir, M. Ashraf, M.A. Al Nasim, F.M. Shah, Brain tumor detection using convolutional neural network, in: 2019 1st International Conference on Advances in Science, Engineering and Robotics Technology (ICASERT), 2019 May 3, pp. 1–6. IEEE.
- [18] V.N. Varghees, M.S. Manikandan, R. Gini, Adaptive MRI image denoising using total-variation and local noise estimation, in: IEEE-International Conference On Advances In Engineering, Science And Management (ICAESM-2012), 2012 Mar 30, pp. 506–511. IEEE.
- [19] T.V. Burrus, C. Burrus, K. Narasimhan, Y. Guo, C. Li, *Introduction To Wavelets And Wavelet Transforms-A Primer*, Burrus CS, 1998.
- [20] B.Q. Chen, J.G. Cui, Q. Xu, T. Shu, H.L. Liu, Coupling denoising algorithm based on discrete wavelet transform and modified median filter for medical image, *J. Cent. South Univ.* 26 (1) (2019 Jan) 120–131.
- [21] S. Paris, P. Kornprobst, J. Tumblin, F. Durand, Bilateral filtering: theory and applications, *Found. Trends® Comput. Graph. Vis.*, 4(1) (2009 Aug 17) 1–73.
- [22] H. Mzoughi, I. Njeh, M.B. Slima, A.B. Hamida, C. Mhiri, K.B. Mahfoudh, Denoising and contrast-enhancement approach of magnetic resonance imaging glioblastoma brain tumors, *J. Med. Imaging* 6 (4) (2019 Oct), 044002.
- [23] R. Riji, J. Rajan, J. Sijbers, M.S. Nair, Iterative bilateral filter for Rician noise reduction in MR images, *SIViP* 9 (7) (2015 Oct) 1543–1548.
- [24] K. Krissian, S. Aja-Fernández, Noise-driven anisotropic diffusion filtering of MRI, *IEEE Trans. Image Process.* 18 (10) (2009 Jun 19) 2265–2274.
- [25] X. Zhang, G. Hou, J. Ma, W. Yang, B. Lin, Y. Xu, W. Chen, Y. Feng, Denoising MR images using non-local means filter with combined patch and pixel similarity, *PLoS One* 9 (6) (2014 Jun 16) e100240.
- [26] J. Yang, J. Fan, D. Ai, S. Zhou, S. Tang, Y. Wang, Brain MR image denoising for Rician noise using pre-smooth non-local means filter, *Biomed. Eng. Online* 14 (1) (2015 Dec) 1–20.
- [27] T. Lu, T. Li, D. Wu, X. Li, Autoencoder Combined with CBAM Improves Denoising of MR Images, in: 2021 11th International Conference on Information Technology in Medicine and Education (ITME), 2021 Nov 19, pp. 209–213. IEEE.
- [28] M.S. Hema, N. Sharma, G. Abhishek, G. Shivani, P. Pavan Kumar, Identification and Classification of Brain Tumor Using Convolutional Neural Network with Autoencoder Feature Selection, in: International Conference on Emerging Technologies in Computer Engineering, Springer, Cham, 2022, pp. 251–258.
- [29] S. Suryanarayana, B.L. Deekshatulu, K.L. Kishore, Y.R. Kumar, Estimation and removal of Gaussian noise in digital images, *Int. J. Electron. Commun. Eng.* 5 (1) (2012) 23–33.
- [30] S. Saladi, P.N. Amutha, Analysis of denoising filters on MRI brain images, *Int. J. Imaging Syst. Technol.* 27 (3) (2017 Sep) 201–208.
- [31] S. Jifara, F. Jiang, S. Rho, M. Cheng, S. Liu, Medical image denoising using convolutional neural network: a residual learning approach, *J. Supercomput.* 75 (2) (2019 Feb) 704–718.
- [32] S. Agarwal, O.P. Singh, D. Nagaria, Analysis and comparison of wavelet transforms for denoising MRI image, *Biomed. Pharmacol. J.* 10 (2) (2017 Jun 20) 831–836.
- [33] K.H. Kim, W.J. Do, S.H. Park, Improving resolution of MR images with an adversarial network incorporating images with different contrast, *Med. Phys.* 45 (7) (2018 Jul) 3120–3131.
- [34] S. Nasrin, M.Z. Alom, R. Burada, T.M. Taha, V.K. Asari, Medical image denoising with recurrent residual u-net(r2u-net) base auto-encoder, in: 2019 IEEE National Aerospace and Electronics Conference (NAECON), 2019 Jul 15, pp. 345–350. IEEE.
- [35] X. You, N. Cao, H. Lu, M. Mao, W. Wanga, Denoising of MR images with Rician noise using a wider neural network and noise range division, *Magn. Reson. Imaging* 1 (64) (2019 Dec) 154–159.
- [36] H.V. Bhujle, B.H. Vadavadi, NLM based magnetic resonance image denoising—A review, *Biomed. Signal Process. Control* 1 (47) (2019 Jan) 252–261.
- [37] D. Sil, A. Dutta, A. Chandra, Convolutional neural networks for noise classification and denoising of images, in: TENCON 2019-2019 IEEE Region 10 Conference (TENCON), 2019 Oct 17, pp. 447–451. IEEE.
- [38] D. Hong, C. Huang, C. Yang, J. Li, Y. Qian, C. Cai, FFA-DMRI: A network based on feature fusion and attention mechanism for brain MRI denoising, *Front. Neurosci.* 16 (14) (2020 Sep), 577937.
- [39] B. Goyal, A. Dogra, S. Agrawal, B.S. Sohi, A. Sharma, Image denoising review: From classical to state-of-the-art approaches, *Inform. Fusion.* 1 (55) (2020 Mar) 220–244.
- [40] M. Tian, K. Song, Boosting magnetic resonance image denoising with generative adversarial networks, *IEEE Access* 19 (9) (2021 Apr) 62266–62275.
- [41] S. Ramesh, S. Sasikala, N. Paramanandham, Segmentation and classification of brain tumors using modified median noise filter and deep learning approaches, *Multimed. Tools Appl.* 80 (8) (2021 Mar) 11789–11813.
- [42] D. Pankaj, D. Govind, K.A. Narayananakutty, A novel method for removing Rician noise from MRI based on variational mode decomposition, *Biomed. Signal Process. Control* 1 (69) (2021 Aug), 102737.
- [43] D. Seelakshmi, S. Inthiyaz, Fast and denoise feature extraction based ADMF-CNN with GBML framework for MRI brain image, *Int. J. Speech Technol.* 24 (2) (2021 Jun) 529–544.
- [44] A. Sharma, V. Chaurasia, MRI denoising using advanced NLM filtering with non-subsampled shearlet transform, *SIViP* 15 (6) (2021 Sep) 1331–1339.
- [45] M. Juneja, S.K. Saini, S. Kaul, R. Acharjee, N. Thakur, P. Jindal, Denoising of magnetic resonance imaging using bayes shrinkage based fused wavelet transform and autoencoder based deep learning approach, *Biomed. Signal Process. Control* 1 (69) (2021 Aug), 102844.
- [46] W. Deren, Z. Fengguang, The theory of Smale's point estimation and its applications, *J. Comput. Appl. Math.* 60 (1–2) (1995 Jun 20) 253–269.
- [47] Q. Huynh-Thu, M. Ghanbari, Scope of validity of PSNR in image/video quality assessment, *Electron. Lett.* 44 (13) (2008 Jun 19) 800–801.
- [48] Z. Wang, A.C. Bovik, H.R. Sheikh, E.P. Simoncelli, Image quality assessment: from error visibility to structural similarity, *IEEE Trans. Image Process.* 13 (4) (2004 Apr 13) 600–612.